1 **EcoTWIN 1.0: A Fully Distributed Tracer-Aided Ecohydrological Model Tracking Water,**

2 **Isotopes, and Nutrients**

3 Songjun Wu[1], Doerthe Tetzlaff[1,2], Yi Zheng[3], Chris Soulsby[4]

4 1 Department of Ecohydrology and Biogeochemistry, Leibniz Institute of Freshwater Ecology and

5 Inland Fisheries, Berlin, Germany

6 2 Geography Institute and IRI THESys, Humboldt University of Berlin, Berlin, Germany

7 3 School of Environmental Science and Engineering, Southern University of Science and Technology,

8 Shenzhen, China

9 4 Northern Rivers Institute, School of Geosciences, University of Aberdeen, UK

10 Corresponding author: Songjun Wu (songjun.wu@igb-berlin.de)

11

Abstract

13 The value of stable water isotopes in constraining process representation in hydrological models is

14 well acknowledged with numerous tracer-aided hydrological models developed in recent years, yet

15 few have leveraged these benefits for more robust water quality modelling. Therefore, we introduce

16 EcoTWIN, a fully distributed tracer-aided ecohydrological model that simultaneously *tracks water*,

17 *isotope*, and *nutrient* fluxes. A thorough model test was conducted by calibrating EcoTWIN against

18 discharge, in-stream isotopes, and NO_3-N concentrations (1980-2024) in 17 large-scale (10^3 - 10^5 km^2)

19 European catchments spanning a wide range of geographic and climatic gradients. Furthermore, three

20 reanalysis products (ERA5 snow depth, MODIS evapotranspiration, and GRACE surface water anomaly)

21 were employed to further validate the capacity of EcoTWIN to reproduce associated but uncalibrated

22 internal water fluxes. Results showed good model performance of both calibrated in-stream targets

23 and uncalibrated internal fluxes in most catchments. Therefore, we conclude that EcoTWIN is a flexible,

24 transferable modelling tool for prediction and process inference in terrestrial ecosystems ranging from

25 boreal to subtropic climates. Constrained by tracer simulations, the model not only captures the

26 celerity, but also the velocity of hydrological fluxes, thus providing spatio-temporally-explicit

27 estimations of water ages and travel times. Such information provides opportunities to bridge

28 catchment hydrology and water quality by linking travel times with biogeochemical processing times.

29 We demonstrate this with a proof of concept using Damköhler Number in nitrogen modelling.

30

1 Introduction

32 The development of ecohydrological models has been accelerating in the recent decades towards

33 frameworks that are more spatially distributed (instead of lumped or semi-distributed) and complex

34 (integrating more ecohydrological processes) (Pechlivanidis et al., 2011; Wellen et al., 2015). A few

35 examples include SWAT (Arnold et al., 2012), HYPE (Lindström et al., 2010), and mHM-Nitrate (Yang

36 et al., 2018), which have been widely applied worldwide. As process-based models, they are used not

37 only as prediction tools for specific variables, but also as learning tools for model inference, i.e., to

38 track the internal states/fluxes from available observations (Wang et al., 2024). This, however, poses
39 challenges due to the considerable uncertainties in model inference.

40 Inference of internal processes is naturally uncertain due to the lack of direct observations, though
41 such uncertainty can be constrained to some extent by rigorous split-sample calibration and validation.
42 The reason we use "somehow" here is based on the fact that most models are calibrated to a minimal
43 number of variables, and 81% of calibrations used data from a single gauge (mostly at a catchment
44 outlet) as reviewed in Wellen et al., (2015). Additionally, from a technical perspective, "equifinality"
45 further adds to the inference uncertainty due to the potential misinformation in data (uncertainty in
46 model forcing and observations) and model structure (the use of simplified, abstract mathematics to
47 simulate real world processes) (Beven, 2006). This can result in inaccurate process representations
48 yielding deceptively good results through error compensation, thus leading to overconfidence in a
49 model's ability to reproduce within-basin dynamics (Wen et al., 2024; Wu et al., 2025a). As
50 acknowledged by the hydrological community, models calibrated solely against discharge at the
51 catchment outlet reflect only the celerity of hydrological systems (pressure wave propagation), yet
52 constituent transport in water quality modelling relies on the velocity (mass flux of the water)
53 (McDonnell & Beven, 2014). Failure to reconcile these differences can lead to questionable process
54 inferences from many ecohydrological and water quality models.

55 One way to strengthen model inference is to include auxiliary data for calibration (Efstratiadis &
56 Koutsoyiannis, 2010). However, there is a paradox in multi-criteria calibration, as on the one hand,
57 more auxiliary data will feed unique information to the calibration process, thus effectively
58 constraining the model behaviour from an ecohydrological perspective; yet on the other hand, it
59 increases the dimensionality of calibration thus resulting in degraded performance or failure of
60 calibration from a technical perspective. The "curse" of dimensionality in ecohydrological modelling is
61 universal for all the commonly used algorithms under both Bayesian and Pareto theories as
62 demonstrated in Wu et al., (2025c). Therefore, modellers should expect the selected auxiliary data to
63 contain as much information as possible (Nearing et al., 2020). For distributed modelling, the auxiliary
64 data should reflect the cumulative contribution of all upstream reaches/regions, rather than variables
65 that are highly dependent on local condition/processes (e.g. point-scale soil moisture and
66 evapotranspiration measurements etc.).

67 Stable water isotopes, in this context, have powerful potential in cumulative flux tracking. As
68 conservative tracers, ^{2}H and ^{18}O are independent of biogeochemical reactions and naturally integrate
69 landscape heterogeneity, thus providing effective constraints on spatially distributed (dis)connections
70 of hydrological flow paths as well as velocity of the hydrological systems which reflect flux-storage
71 interactions (Jung et al., 2025; Tetzlaff et al., 2015). The value of tracers has long been recognised by
72 hydrologists (Hooper et al., 1988), with many tracer-aided hydrological models developed and evolved
73 in recent years from lumped (Birkel et al., 2011; Godsey et al., 2010), to semi-distributed (van
74 Huijgevoort et al., 2016; Nan et al., 2021), and distributed structure (Kuppel et al., 2018; Remondi et
75 al., 2018). However, few attempts have been made to integrate a tracer-aided hydrological structure
76 into water quality modelling (Birkel & Soulsby, 2015; Jung et al., 2025), despite the need being evident

77   for nearly four decades (Neal et al., 1988). Moreover, existing pioneering models are mostly
78   conceptualised/lumped (Benettin et al., 2015; Dick et al., 2015) and/or loosely coupled via external
79   tracer/water quality modules (Pesántez et al., 2023; Yang et al., 2024; Zhang et al., 2020). The external
80   coupling of model chains transfer necessary internal states and fluxes between sub-models (e.g.
81   hydrological fluxes for constituent mixing in water quality or isotopic modules) via online in-memory
82   coupling (instead of offline on-disk coupling), thus significantly increasing the resources consumption
83   in input/output operations. Such model chains, though providing useful scientific insights, can become
84   problematic for large-scale applications owing to the exponential growth in computational and
85   storage requirements. Therefore, there remains a need to develop a fully distributed, computationally
86   efficient ecohydrological model that combines hydrological, isotopic, and water quality simulations.

87   This research gap motivated the development of EcoTWIN, the model that we present in this paper.
88   To our knowledge, the model is one of the first distributed tracer-aided *ecohydrological* models that
89   *tracks water*, *isotopic*, and *nutrient* fluxes simultaneously in a C++-based framework. For a thorough
90   testing of EcoTWIN, 17 large European catchments were selected for calibration against discharge, in-
91   stream isotopes, and NO_3-N concentrations. These catchments span over a wide range of geographic
92   (Alpine to lowland plain) and climatic (from snow-dominated to Mediterranean) gradients. In addition,
93   the robustness of modelled inference on uncalibrated internal fluxes were also compared with three
94   remote sensing products (snow depth, evapotranspiration, and water storage). Given the overall good
95   integrated performance in most catchments, EcoTWIN is presented as an ecohydrological modelling
96   framework applicable for terrestrial ecosystems ranging from boreal to temperate and subtropical
97   climates across a wide range of geographical environments. The subsequent sections are organised as
98   follows: Section 2 and 3 introduce the model structure of EcoTWIN and details in calibration and
99   validation; the model performance is shown in Section 4; in Section 5 we show the advantages of a
100   tracer-aided ecohydrological framework with an example of how water ages bridge catchment
101   hydrology and water quality models; finally, the current limitations and planned future development
102   of EcoTWIN are also discussed.

103

2 Model description

105   EcoTWIN is fully distributed ecohydrological model implemented in C++. The model consists of
106   hydrological, isotopic, and nitrogen modules, which simulate major ecohydrological states and fluxes
107   from canopy to groundwater (Figure 1). Aided by tracer simulations, the model is additionally able to
108   track the water movement vertically and laterally via the calculation of water ages and travel times.
109   For detailed information of model parameters please refer to Table S1.

110

2.1 Hydrological module

112   EcoTWIN follows a typical multi-layer, top-down, bucket-type approach that resolves the water
113   balance sequentially for the vegetation canopy, three soil layers, unsaturated zone, and groundwater.

As the foundation of solute transport, the hydrological module employs a selective disassembly structure with multiple alternative conceptualisations possible for specific important hydrological processes. The configuration can be specified *a priori* based on the goal of modelling and prior knowledge of the studied catchment(s).

2.1.1 Soil properties

Before iterative simulations, soil characteristics are estimated using appropriate pedotransfer functions. Three different alternatives are provided, each of which requires different levels of inputs but all were found to provide robust estimation of soil porosity (θ_s), field capacity (θ_{fc}), wilting point (θ_{wp}), and hydraulic conductivity (Ks). All the soil properties are required for each soil layer/depth. This can be achieved via three alternative options: (i) assigning identical properties across the whole soil column, (ii) calculating separately for each depth based on depth-dependent inputs, or (iii) extrapolating deeper profile characteristics from the top soil properties based on a depth-dependent equation in Maneta & Silverman, (2013).

The distribution of soil types and land use is assigned from raster file in EcoTWIN. This can be specified as a static boundary condition; alternatively, the distributions can also be updated dynamically via a user-specified interval to reflect any temporal changes due to land management.

2.1.2 Vertical fluxes

The vertical fluxes are resolved for storages in the canopy, soil layers, unsaturated zone, and groundwater. The mass balance of canopy storage (ΔC) follows:

$$\Delta C = P - I - Th \tag{1}$$

where P, I, Th are precipitation, interception, and throughfall, respectively. The throughfall is calculated as the exceedance of current canopy storage from the maximum storage calculated by Leaf Area index LAI and a correlation parameter α.

$$C_{max} = \alpha * LAI \tag{2-1}$$

Alternatively, the maximum canopy storage can be estimated with explicit consideration of precipitation intensity (Landgraf et al., 2023):

$$C_{max} = \alpha * LAI * (1 - \frac{1}{1 + SCF * P/(\alpha * LAI)}) \tag{2-2}$$

where SCF is the vegetation cover fraction calculated by LAI and an extinction coefficient (rE) adopted from HYDRUS-1D (Šimůnek et al., 2013):

$$SFC = 1 - \exp(rE * LAI) \tag{3}$$

Then throughfall is calculated as the exceedance of canopy storage from the maximum:

$$Th = (P + C) - C_{max} \; if \; (P + C) > C_{max} \; else \; 0 \tag{4}$$

142　After reaching land surface, throughfall becomes ponding water (S_{Pond}) or snow (S_{snow}) depending

143　on a temperature threshold for separation ($Thre_{SN}$). Snow will melt and recharge the ponding water

144　in warm conditions (air temperature Ta exceed $Thre_{sn}$) following a degree-day model.

$$melt = S_{snow} * min(dd_{min} + dd_{inc} * Th * (Ta - Thre_{SN}), dd_{max}) \tag{5}$$

145　Where dd_{min} and dd_{max} are the minimum and maximum of degree day factor, while dd_{inc} denotes

146　the rate of increase in the degree-day factor per degree Celsius rise in temperature.

147　The available ponding water infiltrates into the top soil layer using Green-Ampt model (Kale & Sahoo,

148　2011; Maneta & Silverman, 2013), with infiltration capacity first calculated as a function of average

149　soil moisture over the hydrologically active depth:

$$I_f = Ks * (1 + \frac{\psi * \theta_s * (1 - (\theta_1 - \theta_{wt})/(\theta_s - \theta_{wt}))}{\theta_1 * d_1}) \tag{6}$$

150　Where θ_1, θ_s, θ_{wt}, and d_1 are the moisture content, porosity, wilting point, and depth in top soil layer;

151　ψ is a parameter representing soil air entry pressure in m. Then potential infiltration (F_p) is determined

152　from the lesser between the available ponding water (S_{pd}) and potential infiltration rate integrated

153　over time before ponding occurs ($I_f * t_p$).

154　The actual infiltration (F) is solved iteratively using the Newton–Raphson scheme:

$$F = \Delta\theta * d_1 = F_p + Ks * w_{Ks} * (\Delta t - t_p) - \psi\Delta\theta * \ln(\frac{\psi\Delta\theta + \Delta\theta d_1}{\psi\Delta\theta + F_p}) \tag{7}$$

155　where w_{Ks} is anisotropy ratio of vertical to horizontal Ks.

156　The soil storage in each layer is conceptualised as two water pools – a gravitational, free-flowing pool

157　and a capillary, soil-bound pool. The two pools are separated based on field capacity (Maneta &

158　Silverman, 2013), and percolation happens when soil storage exceeds the threshold. Three alternative

159　schemes are included in EcoTWIN.

160　In the first scheme, all water in excess of field capacity percolates to deeper layer:

$$Pc_i = (\theta_i - \theta_{fc}) * d_i \tag{8-1}$$

161　where Pc_i, θ_i and d_i depict the percolation, moisture content and depth from/in ith soil layer in m.

162　The second scheme additionally considers the hydraulic conductivity (Ks) following the

163　conceptualisation in SWAT (Arnold et al., 2012):

$$Pc_i = (\theta_i - \theta_{fc,i}) * d_i * (1 - \exp(\frac{-\Delta t * Ks}{\theta_{s,i} - \theta_{fc,i}})) \tag{8-2}$$

164　The third scheme relates percolation to the extent of soil saturation with an exponential parameter β

165　(Kumar et al., 2013; Samaniego et al., 2010):

$$Pc_i = (\theta_i - \theta_{fc,i}) * d_i * (1 - \exp(\beta * \log(\theta_i/\theta_{s,i}))) \tag{8-3}$$

166   For evapotranspiration, soil evaporation and transpiration are estimated separately. The separation

167   of PET is realised by surface cover fraction introduced above:

$$PT = PET * SCF; \quad PE = PET - PT \tag{9}$$

168   Soil evaporation is simulated in the top soil layer based on the soil saturation:

$$Evap_s = PE * \min\left(\frac{\theta_1}{\theta_{fc,1}}, 1\right) \tag{10}$$

169   Transpiration is simulated in all soil layers based on the fractions ($f_{root,i}$) of root density ($D_{root,i}$) in

170   each layer partitioned by soil depth and a parameter (γ_{root}):

$$Tr_i = PT * f_{root,i} * \frac{\theta_1 - \theta_{wp,1}}{\theta_{fc,1} - \theta_{wp,1}} \tag{11}$$

$$f_{root,i} = D_{root,i} / \sum_{j=1}^{m} D_{root,j} \tag{12}$$

$$D_{root,i} = \left(1 - \gamma_{root}^{\left(\Sigma_{j=1}^{m} d_j\right)}\right) - \left(1 - \gamma_{root}^{\left(\Sigma_{j=1}^{i} d_j\right)}\right) \tag{13}$$

171   Channel evaporation is also estimated using Penman equation, which relies on net radiation, wind

172   speed, air pressure, and air temperature as inputs.

173   The last soil layer percolates to an unsaturated storage in unsaturated zone (S_{unsat}). The

174   compartment stores the excess water from soil and percolates either downward to groundwater

175   storage (S_{GW}) or laterally downstream. The percolation to groundwater Pc_{GW} is determined by a

176   weighting parameter p_{GW} as a proportion of unsaturated storage:

$$Pc_{GW} = S_{unsat} * p_{GW} \tag{14}$$

177   Additionally, irrigation is conceptualised in EcoTWIN, which is realised via the water extraction from

178   river or groundwater. The source is determined by the geographic location: for a grid cell with channel

179   network, water is extracted directly from river, and local groundwater is used as irrigation source for

180   non-channel grids. The amount of extraction is estimated from a predefine coefficient for crop water

181   demands (w_{irr}) from which the deficit is calculated for each of the m soil layers.

$$deficit = \sum_{i=1}^{m} \left(\theta_{fc,i} - \theta_{wp,i}\right) * w_{irr} * d_i \tag{15}$$

182   Note that the irrigation can switch to groundwater extraction if river storage cannot fill the deficit.

183

2.1.3 Lateral fluxes

185   In EcoTWIN, grid cells are connected laterally at three levels - surface, unsaturated zone, and

186   groundwater. Note that some models omit the unsaturated storage and directly calculate excess

187   water to drain based on the saturation extent of the bottom soil layer (e.g., EcH₂O-iso, Kuppel et al.,

188 2018). EcoTWIN did not follow this conceptualisation because in reality, the lateral drainage is focused
189 in the saturated zone, and thus the bottom of the soil layer instead of the whole soil profile. The
190 drainage of an entire soil layer thus brings considerable uncertainty to the velocity of lateral transport
191 when the lower boundary of the soil is a parameter to tune in calibration. For instance, a large soil
192 depth will dramatically reduce the velocity of interflow drainage and slow down the mixing of
193 constituents, though this might still perfectly reproduce the celerity (hydrograph) for purely
194 hydrological modelling. Our conceptualisation (an independent unsaturated compartment) aligns
195 with most hydrological models (Arnold et al., 2012; Yang et al., 2018) and fits the recent analysis
196 supporting the dominant role of lateral drainage over vertical transports globally (Mcmillan et al.,
197 2025).

198 By the end of each timestep, ponding water receives upstream inputs and contributes to channel
199 storage if the grid is connected to the channel network, while non-channel grid has $Ovf_C = 0$:

$$Ovf_C = (Ovf_{T,in} + S_{pond}) * p_{Ovf} * dx_C/dx_T \tag{16}$$

200 dx_C and dx_T are the channel length and size of terrestrial grid cell; p_{Ovf} is a weighting parameter for
201 channel recharge. Then the remaining ponding water routes to downslope terrestrial grid following
202 the topographic gradient. In none-channel grid cells, all available ponding storage routes lateral
203 downstream ($Ovf_C = 0$):

$$Ovf_{T,out} = (Ovf_{T,in} + S_{pond}) - Ovf_C \tag{17}$$

204 Similarly, unsaturated storage contributes first to channel storage in grid cells within channel network,
205 while non-channel grid cells have $Inf_C = 0$:

$$Inf_C = (Inf_{T,in} + S_{vadose}) * K_{vadose} * \left(1 - e^{-1*exp_{Inf}*(Inf_{T,in}+S_{vadose})}\right) * p_{Inf} \tag{18}$$

206 where K_{vadose} is the effective conductivity of lateral transport in the unsaturated zone; while exp_{Inf}
207 is an exponential parameter determining the strength of positive correlation between recharge and
208 current unsaturated storage. Then the remaining unsaturated storage is partially routed to downslope
209 grid cell following a linear approximation of Kinematic wave equation, which assumes gravitational
210 flux per unit width $Inf_{T,out}$ is proportional to the subsurface hydraulic conductivity (K_{vadose}) and
211 bedrock slope ($slope$ approximated from the surface slope):

$$Inf_{T,out} = (Inf_{T,in} + S_{unsat} - Inf_C) * \left(1 + \alpha * \frac{dt}{dx}\right) * \alpha * \frac{dt}{dx} \tag{19}$$

$$\text{where } \alpha = K_{unsat} * \sin(slope)$$

212 Groundwater routing is similar to that of interflow, with channel recharge followed by terrestrial
213 transport. Note that the terrestrial groundwater flow does not consider the bedrock slope as
214 groundwater storage is generally much large than unsaturated storage, and thus independent from
215 topographic gradients:

$$GWf_C = (GWf_{T,in} + S_{GW}) * K_{GW} * \left(1 - e^{-1*exp_{GWf}*(GWf_{T,in}+S_{GW})}\right) * p_{GWf} \tag{20}$$

$$GWf_{T,out} = \left(GWf_{T,in} + S_{GW} - GWf_C\right) * \left(1 + \alpha * \frac{dt}{dx}\right) * \alpha * \frac{dt}{dx} \tag{21}$$

where $\alpha = K_{vadose}$

216 The channel routing is realised using Kinematic wave equation based on a scaled channel roughness
217 parameter (Maneta & Silverman, 2013).

218

2.2 Isotopic module

219

220 The isotopic module in EcoTWIN tracks the composition of stable water isotopes in all water storage
221 compartments following hydrological mixing and fractionation. The module also provides estimation
222 of water age and travel time conceptualised as the time since water molecules enter the catchment
223 as precipitation, and the time water molecules need to travel through the specific storage.

224 *2.2.1 Mixing*

225 The mixing and transport of isotopes (^{2}H and ^{18}O, both noted as C) are governed by the velocity of
226 hydrological fluxes with a complete mixing strategy for most water storages:

$$\frac{d(V * C)}{dt} = \sum_{k=1}^{N_{in}} q_{in,k} * C_{in,k} - \sum_{k=1}^{N_{out}} q_{out,k} * C \tag{22}$$

227 Where V and C are the volume and composition/concentration of the storage, while N_{in} and N_{out}
228 denote the number of influx and outflux. Such strategy is built on two assumptions: (i) constitutes (i.e.,
229 isotopes) are fully mixing within each timestep; (ii) the composition/concentration in outflow equals
230 to that in storage. Additional mixing between ponding and upper soil water storage is allowed (with
231 proportion determined by a parameter $SrfMixing$), as nutrients in top soils can be flushed out in
232 large hydrological events (Seybold et al., 2022).

233 The full-mixing assumptions have been widely used and shown to be reasonable for storages with
234 relatively small volumes in many mixing/water quality models (Arnold et al., 2012; Yang et al., 2018).
235 However, some studies show that a complete mixing strategy can be problematic for large storages
236 such as groundwater as they are generally poorly constrained (e.g. Soulsby et al., 2015). Therefore,
237 the mass conservation equation used in the INCA-N model and mHM-Nitrate is employed to calculate
238 the mixing of groundwater storages with influxes (i.e., percolation from unsaturated storage and
239 lateral groundwater inflow).

$$\frac{dC}{dt} = \frac{1}{V + V_r} * \left(\sum_{k=1}^{N_{in}} q_{in,k} * C_{in,k} - \sum_{k=1}^{N_{out}} q_{out,k} * C\right) \tag{23}$$

240 where V_r is the retention storage. The equation is solved by the fourth order Runge-Kutta technique.

241

2.2.2 Fractionation

As conservative tracers, the composition of isotopes in water storages/fluxes is only changed by kinetic fractionation apart from hydrological mixing. The process is accompanied by evaporation, resulting in the preferential loss of lighter isotopes (^{1}H and ^{16}O) to the vapor phase and a corresponding enrichment of heavier isotopes (^{18}O and ^{2}H) in the residual water. In EcoTWIN, the fractionation is simulated along with evaporation of top soil water and river storage based on the Craig-Gordon model (Craig et al., 1964; Kuppel et al., 2018), while transpiration is assumed to be a non-fractionating process (Dawson & Ehleringer, 1991; Kuppel et al., 2018).

$$C = C^* - (C^* - C) * \left(\frac{S - Evap}{S}\right)^m \tag{24}$$

where C^* and m are the limiting isotopic composition (in ‰) and the dimensionless enrichment slop that are estimated via the following equations in (Good et al., 2014):

$$C^* = \frac{h_a C_a + h_s \varepsilon^+ + \varepsilon^k}{h_s - h_a + \varepsilon^k/1000} \tag{25}$$

$$m = \frac{h_a - (h_s \varepsilon^+ + \varepsilon^k)/1000}{h_s - h_a + \varepsilon^k/1000} \tag{26}$$

where h_a is the relative humidity above the soil surface normalised from atmospheric relative humidity (h), air temperature (T_a), and soil temperature (T_s estimated from Amato & Giménez, 2024). C_a is the isotopic composition of ambient air moisture estimated from precipitation composition:

$$C_a = (C_{rain} - \varepsilon^+)/\alpha^+ \tag{27}$$

where ε^+ is the equilibrium fractionation factor (Skrzypek et al., 2015); α^+ is a temperature factor estimated from T_a.

$$\varepsilon^+ = (1 - 1/\alpha^+) * 1000 \tag{28}$$

The factor of diffusion-controlled kinetic isotopic separation ε^k is calculated based on the relative humidity of soil surface (h_a) and soil pore (h_s).

$$\varepsilon^k = (h_s - h_a) * \left(1 - \frac{D_i}{D}\right) * n \tag{29}$$

Where D_i and D denote the diffusivities of water vapor molecules containing heavier isotope and the lighter isotope, respectively. The ratio can be acquired in Horita et al., (2008) for [2]H (0.9877) and [18]O (0.9859). n is an advection term ranging between 0.5 (in saturated soils) and 1 (in dry soils). The factor is included in calibration for the fractionation of top soil evaporation yet fixed as 0.5 for that of channel evaporation.

265 ***2.2.3 Water age and travel time***

266 EcoTWIN can track the age of water i.e., the time since water enters the catchment as precipitation,
267 in each storage. In age tracking, precipitation is defined as new water with age of zero. At the end of
268 each time step, water ages of all storages are advanced based on the temporal resolution (for instance
269 one day if the model is set up for daily timesteps). Note that in some circumstances, the modellers
270 might need to disable the age evolution of specific storage(s) (e.g., groundwater storage) as the
271 storage can be too large to achieve steady states in model spin-up. Similar to isotopes, water ages are
272 only controlled by hydrological transport with the same mixing strategy (i.e., complete mixing except
273 for groundwater).

274 The water ages in EcoTWIN are the mean values averaged from all water molecules in the storage,
275 which might be dominated by the inflow of very old water that obscure the age distribution of the
276 young water (e.g., the groundwater input to top soils due to the groundwater extraction for irrigation).
277 Therefore, EcoTWIN additionally provides the estimation of travel time - the time of water molecule
278 travelling through each storage. The simulation is similar to that of water ages. The only difference is
279 that the transition of water between storges (e.g., percolation into deeper soil layers) resets the travel
280 time to zero. Accordingly, all the water enters a new storage becomes new water instead of just
281 precipitation in water age tracking.

282

283 **2.3 Nitrogen module**

284 The nitrogen module describes the mass balance of nitrogen, particularly nitrate as the main form of
285 dissolved nitrogen, which is dominated by the interaction of hydrological transport and
286 biogeochemical transformations.

287 For each timestep, the nitrate concentration is simulated in each storage following three processes –
288 hydrological transport/mixing, nitrogen inputs, and biogeochemical transformations. Fully integrated
289 with hydrological module, nitrate transport also aligns with hydrological fluxes following the same
290 mixing strategy as in the isotopic simulation. For nitrogen sources, EcoTWIN considers the inputs from
291 fertiliser, manure, and plant residues, whose annual inputs can be specified via configuration. Notably,
292 fertilization can be parameterised via spatial raster inputs if corresponding dataset is available. The
293 timing and extent of nitrogen addition of all sources are determined following the implementation in
294 HYPE (Lindström et al., 2010), which distributes the annual sum across a specified period (e.g., the
295 period between planting and harvest for crops). Additionally, wet deposition is conceptualised as the
296 atmospheric nitrogen source, whose concentration can be specified via spatial raster and simply as a
297 constant value.

298 The biogeochemical transformations are mainly modified from the mHM-Nitrate model (Yang et al.,
299 2018), and the HYPE model (Lindström et al., 2010), which are conceptualised for the soil profile and
300 channel network. In the soil profile, three nitrogen pools are conceptualised for each soil layer,
301 including an inactive nitrogen pool (SN_i), an active nitrogen pool (SN_a), and a dissolved nitrate pool

(DN). The soil transformations include degradation (Dgd_s, from SN_i to SN_a), mineralisation ($Minr_s$, from SN_a to DN), denitrification ($Deni_s$, from DN to gaseous N₂), and plant uptake ($Uptk_s$, DN removal).

$$Dgd_s = SN_i * ref_{Dgd,s} * f_{Ta} * f_\theta / dt \tag{30}$$

$$Minr_s = SN_a * ref_{Minr,s} * f_{Ta} * f_\theta / dt \tag{31}$$

$$Deni_s = DN * ref_{Deni,s} * f_{Ta} * f_{\theta,deni} * f_{conc,s} / dt \tag{32}$$

where $ref_{Dgd,s}$, $ref_{Minr,s}$, $ref_{Deni,s}$ are the parameters representing the reference rates of soil degradation, mineralisation, and denitrification. f_{Ta} and f_θ are the regulating factors of temperature and moisture.

$$f_{Ta} = 2^{(T_a-20)/10} * \omega \quad where\ \omega = \begin{cases} 1 & T_a > 5 \\ T_a/5 & 0 \le T_a \le 5 \\ 0 & T_a > 0 \end{cases} \tag{33}$$

$$f_\theta = min\left[\frac{(1 - p_{\theta,deni}) * (\theta_{fc,i} - \theta_i)}{p_{\theta,fc} * d_i}, \frac{(\theta_i - \theta_{wp,i})}{p_{\theta,wp} * d_i}\right] \tag{34}$$

where $p_{\theta,fc}$ and $p_{\theta,wp}$ are the empirical factors that are fixed as 1.2, 0.8 based on literature values (Lindström et al., 2010; Yang et al., 2018). $p_{\theta,deni}$ is the saturation threshold for soil denitrification ranging between $0.4 - 0.85$ (Yang et al., 2018). A different moisture factor considering a saturation threshold (θ_{thres}) is employed for denitrification, as denitrification is more sensitive to the soil wetness condition:

$$f_{\theta,deni} = \left[(\theta_i/\theta_{fc,i} - \theta_{thres})/(1 - \theta_{thres})\right]^{2.5} \tag{35}$$

The process is additionally controlled by the concentration level in the storage $f_{conc,s} = C/(C + 10)$. Plant uptake is simulated using a three-parameter logistic growth equation in (Eckersten et al., 1994; Lindström et al., 2010).

Currently, in-stream denitrification is the only process considered in EcoTWIN.

$$Deni_w = ref_{Deni,w} * f_{T_w} * f_{conc,w} * A / dt \tag{36}$$

where $ref_{Deni,w}$ is the reference in-stream denitrification rates. The actual rates are regulated by a concentration factor $f_{conc,w} = C/(C + 1.5)$ and a temperature factor f_{T_w} (the same equation for f_{Ta} with inputs substituted by river temperature f_{T_w}, simplified as the rolling-average of 20-day air temperature).

It should be noted that the calibrated soil depth in this study is about 2.5 m, with intermittent saturation occurring in the deeper layer. This means that terrestrial denitrification is a combination of soil and groundwater processes in this study, though this might change in other applications if a shallow soil depth is assigned.

3 Model calibration and validation

A robust model application should not only reproduce observed variables through calibration but also yield realistic estimates of internal states and fluxes that are not included in the calibration process. This is essential to avoid situations where inaccurate process representations produce deceptively good results through error compensation. Therefore, we evaluate EcoTWIN from both perspectives. First, we assess the model's ability to reproduce observations via calibration (methods and results in Sections 3.2 and 3.4). Then, we examine the model's capacity to simulate uncalibrated internal states and fluxes by comparing the simulated snow depth, evapotranspiration, and total water storage with corresponding remote-sensing products (methods and results in Sections 3.3 and 3.5).

To ensure model generality, 17 catchments were selected for calibration and validation depending on the data availability (particularly stream stable water isotopes and nitrate), which span a wide range of characteristics in geography, climate, and anthropogenic managements (Figure 2 and Table 1). Anthropogenic management practices have a less dramatic effect than climate and geography in most catchments due to the relatively low proportion of urbanized areas. However, a few notable exceptions—such as the Rhine, Elbe, and Danube catchments—are included in the analysis, as these densely populated regions hold critical ecological, agricultural, and economic importance for Europe, and are subject to intensive human interventions in water management. This also provides a chance to examine the applicability of EcoTWIN in human-affected catchments.

3.1 Model setup

EcoTWIN was setup for each of the 17 catchments for calibration with a spatial resolution of 5 km^2 and a temporal resolution of daily timesteps from 1980 to 2024 (with first two years for spin-up). As a fully distributed model, gridded GIS inputs are used in the model setup, including a digital elevation model, flow direction, slope, channel width, channel length, proportion of each land use type (Winkler et al., 2021), proportions of each soil type (world soil map, WRB2014), and soil properties (e.g., depth-dependent proportions of clay, sand, silt, and organic matter from SOILGRIDS). All spatial inputs were acquired with finer resolution (50 m or above) and resampled to the resolution of this application (5 km).

The climatic variables used to drive EcoTWIN include precipitation, air temperature, potential evapotranspiration, relatively humidity, and a few variables that are optional required for the calculation of channel evaporation (air pressure, net radiation, and wind speed). These climatic variables are available from the reanalysis products ERA5 and E-OBS, while PET is calculated using FAO Penman-Monteith equation. For nitrogen simulations, additional inputs are needed including the fertilization map (Grizzetti et al., 2021) and nitrate concentration of rainfall (Zhu et al., 2025) as the boundary of nitrogen addition from agricultural activities and wet deposition.

3.2 Model calibration

The calibration was conducted separately for each catchment to test the applicability of EcoTWIN under different geological and climatic contexts. Three commonly used variables for hydrological and water quality modelling (discharge, stream water isotope composition, and in-stream NO_3-N concentrations) are employed for calibration. Their long-term time series were acquired at daily steps from different sources (discharge from GRDC, isotopes from Wateriso and GNIR, and NO_3-N concentration from global water quality database, GEMStat), and then compared with simulation results at multiple sites for each catchment. Here ^{18}O was selected for isotopic validation due to its higher precision and data abundance. Given the discrepancy in duration of observations (especially for isotopes and NO_3-N), a separate calibration and validation based on a split-sample approach is difficult. Therefore, the full timescale (1982 - 2024) was used for calibration (and the validation introduced in Section 3.3).

The DiffeRential Evolution Adaptive Metropolis algorithm (DREAM) was selected for parameter optimisation due to its relatively efficient and effective performance for high-dimensional problems (as benchmarked in Wu et al., 2025c). The algorithm was implemented separately for each catchment with the same prior distribution of parameters (Table S1). The maximum iteration was set as 100,000 for each catchment (20 chains with maximum chain length of 5000), from which 40 best simulations were selected from the posterior distribution. The Kling-Gupta efficiency (KGE) statistic was used to construct an informal likelihood function for DREAM optimisation.

$$l = \left[\sum_{i=1}^{N_{obs}} \sum_{j=1}^{N_{site}} (1 - KGE) * w_{i,j} \right]^{-m} \tag{37}$$

Where l is the likelihood; N_{obs} and N_{site} are the number of observation types (discharge, isotopes, and nitrate) and sites. The weight $w_{i,j}$, defined for observation type i at site j, is assigned equally across sites such that the total weight for each observation type sums to 1/3. m is an exponentially coefficient to stretch the likelihood surface that is often set based on the number of observation points. After prior test run, m was set as 500. Finally, the likelihood function is transformed to logarithmic form for numeric stability. The calibration was validated using Kling-Gupta efficiency (KGE), Root Mean Square Error (RMSE), Pearson Correlation Coefficient (Coefficient), and Percent bias (Pbias) (Table 2).

3.3 Model validation

Reanalysis products were further employed to validate uncalibrated internal model states or fluxes from three important perspectives in ecohydrological modelling – snow depth from ERA5, evapotranspiration from MODIS, and surface water mass anomaly from GRACE (as a storage proxy). The simulated variables corresponding to these products are, respectively, the depth of snow pack, the sum of soil evaporation, channel evaporation, and transpiration from all soil layers, and the anomaly of total water storage above groundwater (i.e., the sum of canopy storage, snow, soil water storages, and unsaturated storage). The validation was realised via resampling the remote sensing

397 products to 5 km and comparing grid-to-grid with the modelled outputs. Note that r^2 was used as the
398 performance metrics, as KGE is not applicable for time series with zero average, yet the average of
399 surface mass anomaly is close to 0.

400

3.4 Calibration performance

402 EcoTWIN successfully reproduced the observed discharge in all 17 catchmes with KGE exceeding 0.5
403 at most site (Figure 3a). This is further demonstrated in Figure 4 where both seasonality and peaks of
404 discharge with different levels of magnitudes were captured. Such performance is at least comparable
405 to or better than previous continental calibration of hydrological models (e.g., ParFlow, Naz et al.,
406 2023; E-HYPE, Donnelly et al., 2016).

407 Similarly, isotopic and nitrate simulations also produced good performances at most sites (Figure 3b).
408 However, there are a few exceptions. The failure of isotopic simulations was found at two sites within
409 the Alphine region (bottom left corner of figure 3b). This can be attributed to the uncertainty in
410 precipitation isotopes and snowmelt isotopes (due to the lack of snow elusion fractionation; Ala-aho
411 et al., 2017), the incorrect isotopic composition in groundwater, or the reduced applicability of degree-
412 day model for mountainous areas in Europe. Such simulation deviation due to the uncertainty in data
413 and boundary initialisation is often reported in previous calibration (Smith et al., 2021).

414 In general, the model produces comparable performances to existing nitrogen modelling at catchment
415 (Wu et al., 2022, 2025b; Yang et al., 2018) and continental scales (Jones et al., 2023; Mikayilov et al.,
416 2015). However, nitrate simulations failed to capture the observations at three sites, though as is
417 shown in Figure 4, these all have relatively low levels of NO_3-N concentrations. Such low average
418 values can easily trigger the degradation in KGE as one of the sub-components of KGE is highly
419 sensitive to the mean deviation, though the absolute deviation remained low (Figure 4, Table 2).
420 Overall, we concluded that EcoTWIN has good capacity to reproduce in-stream components for a wide
421 range of catchments and for relatively long periods.

422

3.5 Validation performance

424 Apart from the variables used for calibration, three internal states and fluxes are also compared with
425 remote sensing products. First, the sum of soil evaporation, channel evaporation, and transpiration
426 was compared to MODIS evapotranspiration in each grid cell. The results in Figure 5 shows a general
427 good fit between simulation and observation with r^2 above 0.5 in most regions. From the subplots in
428 Figure 5, we can see that the seasonality and magnitude of evapotranspiration were well captured
429 though the peaks in summer were slightly underestimated.

430 Then, the water storage anomaly was compared to the anomaly of simulated surface storage, i.e., the
431 sum of canopy storage, snow, soil water storages, and unsaturated storage. The grid-to-grid
432 comparison in Figure 6 shows a general good fit in most regions with r^2 close to or above 0.5. However,
433 more degradation was found compared to the performance in evapotranspiration, especially in

coastal regions. For instance, GRACE exhibited considerably increasing trends in water storage between 2005 to 2015 in two Nordic catchments (W2 and W3), yet our simulations only showed a moderate increasing trend. Similar degraded performance was found in the coastal catchments (e.g., three British catchments W6-8 in UK), though the magnitudes of simulation and observations fit well. This is possibly attributed to the coarse resolution of GRACE which additional considered the storage mass from ocean in coastal region yet not included in this terrestrial-explicit modelling.

Finally, the simulated snow depth was compared to the daily snow depth in ERA5 reanalysis products (ERA5 post-processed daily statistics on single levels; 10.24381/cds.4991cf48). Results in Figure 7 show a good agreement between simulations and ERA5 records in most regions with r2 > 0.5, though degradation was found in a few catchments. Note that, the poor performances were generally found in catchments with limited snow accumulation, e.g., W14-17 in subplots in Figure 7. In the other words, the absolute deviation was relatively limited for snow depth simulation.

4 Water age simulation and its link to water quality

Like many existing distributed hydrological and water quality models (e.g., SWAT, mHM, EcH$_2$O-iso, HYPE etc.), EcoTWIN can provide estimation of the main ecohydrological fluxes at high spatial and temporal resolutions, including canopy interception, snow melt-accumulation, infiltration, percolation through soil layers, groundwater recharge, and lateral flux routing at different horizontal phrases. Among these variables, a unique trait of EcoTWIN lies in its capacity to track water fluxes via isotopes, thus being able to provide a consistent estimate of water age and travel times. Therefore, in Figure 8, both variables are shown as the long-term average from 1982 to 2024 for soil profile and stream water.

Generally, the magnitudes of water ages follow the geographic and climatic gradients, with younger water found in catchments with higher annual precipitation inputs. Those regions locate in the north-west coast of Europe (Figure 2), particularly for Nordic catchments where lower temperature and net radiation further limit the level of potential evapotranspiration, leading to larger percolation to deeper soil layers and groundwater. Such high turnover rates of water in these catchments (W1, W2, W3, W4, W5, and W8) are also demonstrated as the simulated travel time in soil profile with average values remaining below 500 days.

A similar pattern was also found in mountainous regions with higher precipitation and lower potential evapotranspiration compared to lowland areas. Two clear examples are W12 and W17 located in the Alps and the Taurus Mountains where water ages and travel time remained below 500 days (Figure 2). In specific wet periods, the water ages and travel time can be reduced to just days, suggesting the rapid response of saturated hydrological systems (e.g., the wet year 1999 in Europe in Figure S1-S3). In contrast, the lowlands in central-west Europe showed much slower turnover rates, with the mean water ages reaching almost 10 years in some specific regions. A few examples could be found in the three major representative catchments in Central Europe – Elbe, Rhine, and Danube (W9-11). Such old water ages and long travel time are further exacerbated during dry years (e.g., 2004, a drought year for much of Europe shown in Figure S1-3).

Note that though water ages and travel time share similar magnitudes and spatial patterns. It is partly attributed to the fact that the travel time in the conceptualised storages increases exponentially in a sequential order. Taking the Rhine as an example, the average travel time in top soil layer, median soil layer, deep soil layer are 65, 225, 1291 days, respectively. Such a depth-dependence profile makes the overall ages/travel time follow the magnitude of bottom layer and leads to similarity between water ages and travel time. However, large discrepancies are possible between the two indices if a shallow lower boundary is adopted.

The estimation of travel time and water ages further provides opportunities to link hydrology and water quality processes in the modelling framework. The simplest and most intuitive way is to compare travel times and simulated biogeochemical process kinetics. Taking denitrification as an example, we applied linear regression and Spearman's correlation test to investigate the potential correlation between travel time of soil water and denitrification rates. The results in Figure 9 showed the strong positive correlations in most agricultural-dominated catchments (W5, W5, W6, W8, W9, W11) yet only weak or no correlation in remaining pristine watersheds. This suggests that travel time might be a key control on soil nitrogen removal in European croplands.

More insights can be gained via examination of the Damköhler Number, which quantifies the ratio between timescales of solute transport and biogeochemical transformation. Here in our modelling framework, it can be calculated as the ratio between the travel time of soil water and the time for all soil NO_3-N storage to be removed under the simulated denitrification rates. Damköhler numbers <1 mean that soil water nitrogen cannot be fully removed during time of residence, indicating the dominance of transport over removal processes and the potential of nitrogen leaching. As shown in Figure 10c, the long-term averages of Damköhler number remain below 1 in most croplands, supporting the conclusion from the linear regression (travel time is a major limiting factor on soil nitrogen removal). Via the spatial- and temporal-explicit estimation of Damköhler number, EcoTWIN provides the opportunity to bridge the catchment hydrological and water quality with travel time.

5 Discussion

5.1 Structural and Functional Merits of EcoTWIN

As a new tracer-aided ecohydrological model, EcoTWIN has novel advantages compared to previous models. In this section, we briefly introduced the merits in model structure, applicability, and insights from tracer-aided simulation.

5.1.1 Integrated C++ framework

Applications of large-scale modelling have been increasingly popular due to the accelerating development of observation networks and availability of remote sensed data. However, it severely increases the computational burden of ecohydrological modelling. Especially for fully distributed models, increasing size of the model domain can lead to exponential increase in computation demands. In this context, an integrated framework in C++ can significantly accelerate the modelling tasks, as all

509 computation can be conducted within memory thereby avoiding the additional input/output
510 overhead associated with disk-based operations in loosely coupled model chains (e.g., EcH$_2$O-iso-
511 nitrate; Yang et al., 2024). A standard test was not performed, but based on our modelling experience
512 in the same catchment with different models, the speed of EcoTWIN (~5 seconds for a simulation with
513 285 grid cells and 30 years at daily timestep) is close to the water quality model mHM-Nitrate (~5
514 seconds yet without isotopic simulations; Wu et al., 2022) and easily outperforms EcH$_2$O-iso-nitrate (7
515 minutes; Wu et al., 2025b).

5.1.2 Selective disassembly structure

517 EcoTWIN incorporates a wide range of ecohydrological processes from canopy to groundwater, which
518 not only include natural processes but also anthropogenic activities like irrigation. Land managements
519 can also be represented by dynamic parametrisation, thus enabling EcoTWIN to function as a learning
520 tool to investigate the impacts of changes in anthropogenic management over natural ecosystems;
521 for instance, the land use distribution was updated every 10 years in our test examples to reflect the
522 moderate increases in afforestation in the past 45 years in Europe. More importantly, unlike hard
523 coded process representations/equations in most ecohydrological models, EcoTWIN has a selective
524 disassembly structure, which provides alterative conceptualisations for several important hydrological
525 processes (canopy interception, percolation, groundwater recharge, as well as three pedotransfer
526 functions for initialising soil properties). Modellers can benefit from such flexible model structures by
527 either selecting process representations best suited to field knowledge or data prior to calibration, or
528 integrating module selection into the calibration thus enabling simultaneous optimisation of model
529 structure and corresponding parameters. The latter aspect, i.e., the optimisation of model structure,
530 can be realised together with the recently developed optimisation algorithm DREAM$_{(LOAX)}$ that aims to
531 identify the deficits in model structure during calibration (Wu et al., 2025a).

5.1.3 Transferability to contrasting geographic and climatic contexts

533 To thoroughly test the applicability of EcoTWIN, 17 catchments with different climatic and
534 geographical contexts were selected for calibration and validation, spanning over most biomes in
535 Europe, from snow-dominated watersheds in Nordic or alpine regions, to agricultural-influenced
536 lowlands catchments, and Mediterranean ecosystems (Figure 1 and Table 1). Through multi-criteria
537 calibration against three objectives at multiple sites, the model successfully reproduced the
538 seasonality and peaks of discharge, in-stream isotopes, and NO$_3$-N concentrations in most catchments.
539 Such performance is comparable or better than the previous model benchmarks at similar scales
540 (Bajracharya et al., 2023; Mikayilov et al., 2015; Rakovec et al., 2016, 2019). Note that the
541 concentration of NO$_3$-N was used for calibration, whose accurate simulation is more difficult than NO$_3$-
542 N loads given the naturally good performance in discharge. In the other words, hydrological simulation
543 is often the least problematic part in integrated water quality modelling, as it is mostly dominated by
544 natural catchment properties while nitrogen cycling is more interfered by anthropogenic
545 managements (e.g., fertilization and irrigation) (Wu et al., 2025b). Additionally, the simulated internal
546 fluxes were also compared to three reanalysis products in hydrological simulations, corresponding to

547 the key fluxes or storage states in hydrological cycling (snow melt-accumulation, evapotranspiration,
548 and water storage). The results show that constrained by isotopes, EcoTWIN was able to reproduce
549 comparable hydrological modelling results to the remote sensing observations without direct
550 calibration regarding magnitudes, spatial patterns, and temporal dynamics. The only degraded
551 performance was found in GRACE surface mass anomaly in coastal regions. There are two potential
552 reasons: (i) the coarse resolution of GRACE might account for mass shifts in both ocean and land, yet
553 EcoTWIN only produces mass anomaly in terrestrial systems; (ii) bidirectional fluxes across the land-
554 ocean interface might drive key changes in coastal systems, which is not considered in current version
555 of EcoTWIN. Nonetheless, given the relatively good agreement with most available observations, we
556 conclude that EcoTWIN is applicable across a range of terrestrial ecosystems from boreal to temperate
557 and subtropical climate.

558 ### *5.1.4 Bridging hydrology and water quality with water ages*

559 Further to the inference of hydrological and nitrogen processes that is also available in other
560 distributed water quality models (Wellen et al., 2015), a unique trait of EcoTWIN lies in its capacity to
561 track water fluxes and ages with stable water isotopes. As a tracer-aided model, EcoTWIN not only
562 simulates the celerity of catchment response, but tracks the velocity of water via different flow paths.
563 The importance of delineating flow paths within catchments has long been recognized by hydrologists,
564 and has motivated the development of many indices to describe the movement of water molecule at
565 catchment-scale and estimate associated timescales (Sprenger et al., 2019). A few examples are water
566 ages, transient time distribution, and young water fractions (Benettin et al., 2015; Hrachowitz et al.,
567 2013; Jasechko et al., 2016). However, those indices are mainly calculated in a lumped manner where
568 different flow paths in the catchment are characterised as a black box, thus characterising the overall
569 input-output dynamics yet potentially omitting important spatio-temporal variability of hydrological
570 boundary conditions. Instead, EcoTWIN, benefiting from the gridded-based structure, can utilise the
571 increasingly available spatial information (e.g., gridded remote sensing datasets) thus characterising
572 the water ages and travel time in a spatially-explicit manner. Note that simulations of water age/travel
573 time, like other ecohydrological processes, are sensitive to spatial resolution. The coarse resolution
574 used for large catchments (e.g., 5 km in this study) may obscure the sub-grid heterogeneity. For
575 instance, local hydrological hotspots characterized by short travel times and young water ages can be
576 damped or averaged out at coarser resolutions, as reported in modelling studies using EcH2O-iso
577 (Smith et al., 2021; Yang et al., 2023b). However, this limitation can be mitigated by increasing spatial
578 resolution, and it does not undermine the utility of EcoTWIN for water-tracking.

579 Compared to water age which quantifies the age of water within the overall system, travel time,
580 accounting for the water age within a specific storage, is more important in understanding the links
581 between hydrological and nutrient cycles. Such an index, also known as transit time or exposure time,
582 forms one of the fundamental components of water quality modelling. Therefore, the travel time
583 estimated by EcoTWIN has potential to improve the simulation of biogeochemical transformations in
584 water quality models interfaced with simplified hydrological modules (e.g., MONERIS; Bonchkovskyi
585 & Osadcha, 2024). Moreover, travel time can be used as a proxy to bridge hydrological processes and

biogeochemical transformations. Here we presented a simple framework to calculate the Damköhler Number for denitrification. By using the simulated travel time and reaction timescale (i.e., the time for full removal of nitrogen storage under current denitrification rates), estimation of Damköhler Number was achieved in a spatially- and temporally-explicit manner (Figure 9), which can highlight where and when soil nitrogen removal is constrained by the limited exposure time in the catchment. Such high-resolution information is unique, as the use of this index has been largely restricted to steady-state groundwater systems or riparian/hyporheic zones due to the difficulty in quantifying processing time and residence time at larger scales (Ocampo et al., 2006; Wu et al., 2022).

5.2 Limitations and roadmap for future development

Despite these advances, EcoTWIN has limitations. In this section, the uncertainties in model structure and conceptualisation are introduced, as well as the potential roadmaps for future developments.

5.2.1 Potential towards physics-based conceptualisation of groundwater

Groundwater in EcoTWIN is characterised as two conceptual storages linking with adjacent upstream and downstream storages following the topographic gradients. Such conceptualisation, although has been widely employed in hydrological models (e.g., SWAT, mHM, EcH$_2$O, STARR, etc.), does not align with the physical mechanisms of groundwater routing, as groundwater flow direction follows the hydraulic gradients which may not entirely coincide with topographic gradients (Condon et al., 2021). Such simplified routing has less effect in large catchments with clear topographic gradients (e.g., Rhine starting from Alps to North plain), yet might cause biased estimation in water mass balance for flatter headwater catchments (Yang et al., 2025). Therefore, we plan to further incorporate an additional groundwater module to realise physics-based routing following Darcy's Law in future.

5.2.2 Revisiting mixing strategies

Mixing strategy is a key component in water quality or tracer models describing the flux-storage behaviours along specific flow paths. There has long been a debate on different mixing assumptions and theories. A typical example is the two-water-world hypothesis, where water storage in the soil profile is differentiated into a tightly-bound pool and a mobile-water pool (McDonnell, 2014). Such conceptualisation is close to the definition of soil matrix flow and preferential flow: the existence of free-flowing preferential flow will bypass the soil matrix vertically and accelerate the lateral drainage via direct connection with channel network (Hrachowitz et al., 2013; Sprenger et al., 2019). However, a complete mixing strategy is often regarded as a reasonable first approximation in many situations and is used in most water quality and tracer models (Jung et al., 2025). This is not only attributed to its computational simplicity, but also the difficulty in conceptualising preferential flow in an evidenced-based manner. In the other words, even with the recognition of preferential flow, its calculation is often hindered by the subsurface heterogeneity in soils and bedrock; a good visualisation is given in Figure 7 in Sprenger et al., (2019). Alternatively, partial mixing has been developed for ecohydrological models (e.g., Hrachowitz et al., 2013), which could be added as a complementary

19

623 mixing strategy in EcoTWIN. However, as benchmarked in Hrachowitz et al., (2013), the partial mixing
624 brings only moderate improvements in simulations yet can introduce challenges to model spin-up (the
625 increasing instability of storage ages due to the exchange between bypass and storage compartment).
626 Moreover, the realisation of partial mixing, like preferential flow, relies on additional parameters to
627 describe the timing and extent of mixing thus introducing additional parametric uncertainty.
628 Therefore, we recommend a rigorous evaluation of the necessity of partial mixing before any
629 application.

5.2.3 Complementing the in-stream biogeochemical processes

631 Transformation is as crucial as transport in inland-water nitrogen cycling (Wang et al., 2024). In the
632 current version of EcoTWIN, denitrification is the only in-stream process of nitrogen loss. However,
633 recent studies have shown that other processes are involved which may be important for aquatic
634 nitrogen cycling. An example originates from Wang et al., (2024), where global inland-water modelling
635 shows that in-stream denitrification only accounts for a minor fraction of NO_3-N removal compared to
636 biological uptake. Though their modelling considers lakes and reservoirs where primary production of
637 benthic plants and algae is usually greater than that in rivers, in-stream assimilation might still play a
638 significant role, particularly, in slow-flowing river systems. This is supported by a recent modelling
639 study that estimated nitrogen retention at 15-min interval based on high-frequency NO_3-N data (Yang
640 et al., 2023a). Therefore, we plan to further compliment EcoTWIN with in-stream assimilation
641 conceptualisation, as well as other potentially important riverine processes (e.g., nitrogen burial in
642 sediments; Akbarzadeh et al., 2019).

5.2.4 Integrated calibration framework to embrace equifinality

644 Strictly speaking, equifinality is not specifically linked to EcoTWIN, but remains a universal problem for
645 calibration or parameter tunning for almost all ecohydrological models. It is reflected in multiple
646 parameters sets yielding similarly good model performance, thus increasing the uncertainty in process
647 inference. The extent of equifinality is primarily controlled by the magnitude of parameters and
648 observation/objectives (Wu et al., 2025c). Unfortunately, conceptualisations across diverse process
649 domains (e.g. for hydrology, isotopes and N-cycling) in EcoTWIN also lead to a relatively large number
650 of parameters. Such risk in equifinality can be potentially constrained via sensitivity analysis, but can
651 still remain an issue given the ubiquitous epistemic uncertainty in data and model structure (Beven,
652 2006, 2015). Alternatively, the recently developed calibration algorithm $DREAM_{(LoAX)}$ provides an
653 opportunity to embrace equifinality by tunning parameters based on the limits-of-acceptability theory
654 under the equifinality thesis (Wu et al., 2025a). The integrated modelling framework of EcoTWIN and
655 $DREAM_{(LoAX)}$ can potentially increase the robustness of model calibration and inference.

656

6 Conclusions

658 Uncertainty is a central concern in ecohydrological modelling, as models are not only used for
659 prediction of specific variables, but also for process inference (backtracking internal processes from

available observations) that are inherently embedded within considerable uncertainty. Stable water isotopes can help effectively constrain hydrological fluxes due to their conservative nature, motivating the increased development of tracer-aided models. However, few attempts have been made to incorporate a tracer-aided hydrological framework into water quality models.

Therefore, we introduced EcoTWIN, a fully distributed tracer-aided *ecohydrological* model that *tracks water*, *isotopic*, and *nutrient* fluxes simultaneously in an integrated C++-based framework. To thoroughly validate the model, 17 large European catchments were selected with a wide range of geographic and climatic gradients (from snow-dominated watersheds in Nordic or alpine regions, to agricultural-influenced lowlands catchments, and Mediterranean ecosystems). The model was calibrated against long-term observations of discharge, in-stream isotopes, and NO_3-N concentrations during 1980-2024 in each of the 17 catchments. Additionally, uncalibrated internal states and fluxes were also compared with three remote sensing products (ERA5 snow depth, MODIS evapotranspiration, and GRACE surface water anomaly) to validate the credibility of process inference.

The generally good agreements in both calibrated in-stream components and uncalibrated internal flux-states demonstrated that EcoTWIN is a transferable, flexible prediction and learning tool for process inference across biomes ranging from boreal to subtropical climate. Constrained by tracer simulations, the model not only reproduces the celerity of hydrological systems, but also tracks the velocity. Water ages and travel time are embedded in EcoTWIN to provides spatio-temporal-explicit insights into *when*, *where*, and *how* water moves in the system. Such indices further provide the opportunities to efficiently bridge hydrology and water quality at large catchment-scales. An example was presented using the Damköhler Number to identify regions where denitrification was limited by fast turnover rates of water.

Following this "proof of concept" we also see numerous areas where future developments can improve the limitations in the 1.0 version of the model.

Code and data availability

Author contribution

Conceptualization: SW, DT, YZ, CS

Data curation: SW

Methodology: SW
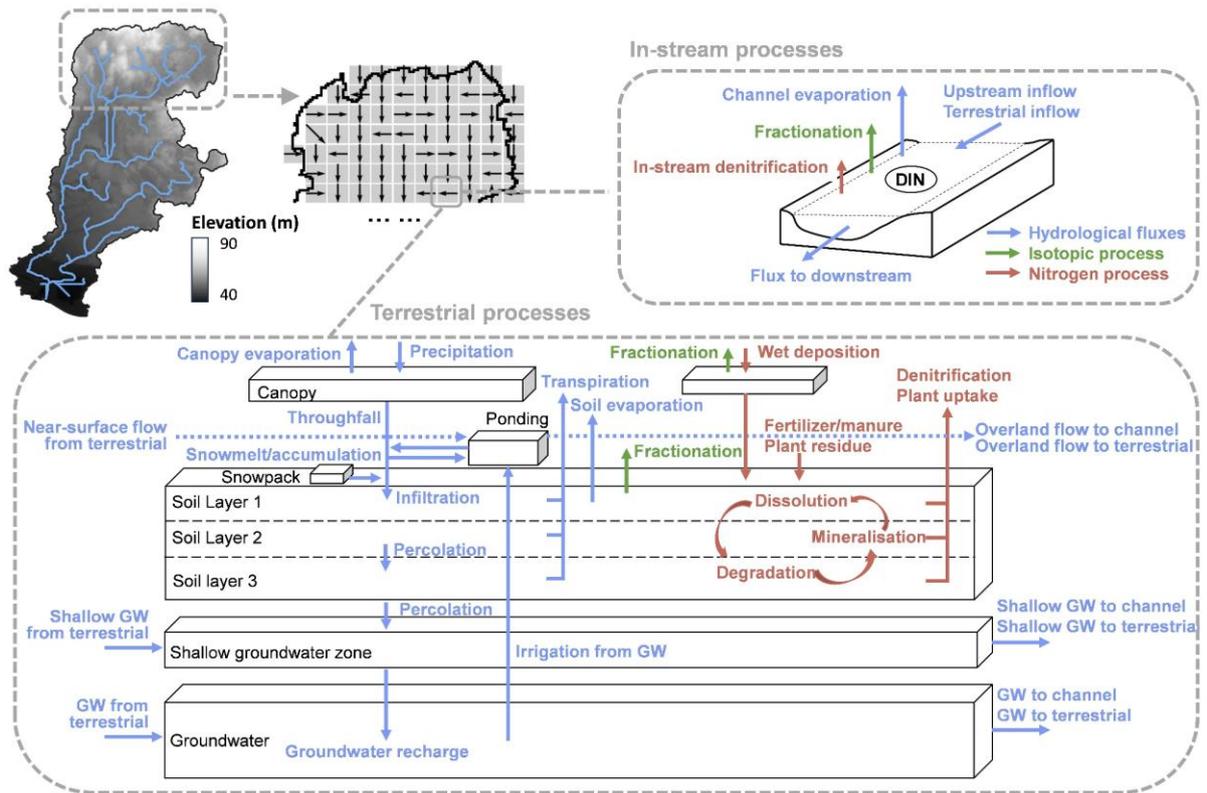
Software: SW

Investigation: SW, DT, YZ, CS

Visualization: SW

Supervision: DT, CS

Writing (original draft preparation): SW

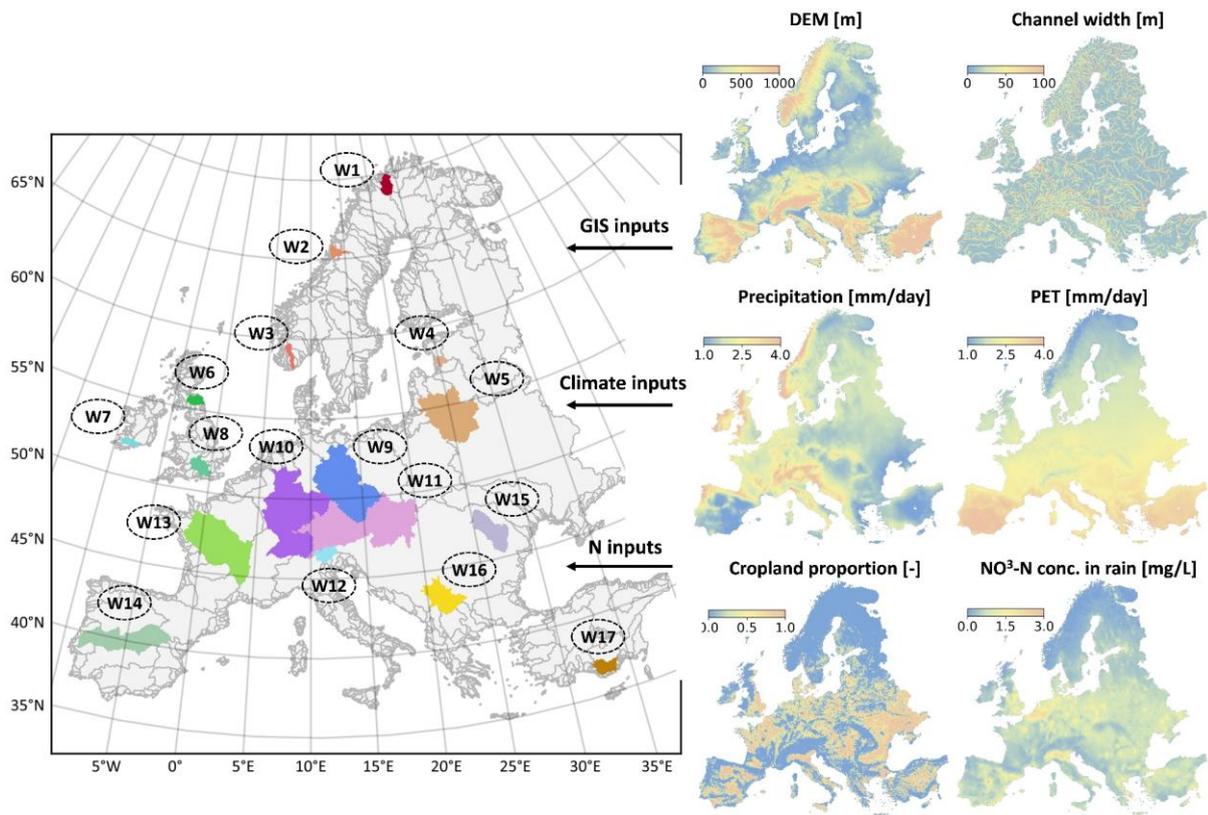Writing (review and editing): SW, DT, YZ, CS

Figures

719

720 Figure 1. Model structure of EcoTWIN. As a distributed model, EcoTWIN disentangles the spatial
721 domain into grid cells. In each grid cell, hydrological, isotopic, and nitrogen processes were simulated
722 in canopy, snow, soils, shallow groundwater, groundwater, and channel.

723

724

725

726   Figure 2. The selected catchments for model validation and an overview of key inputs.
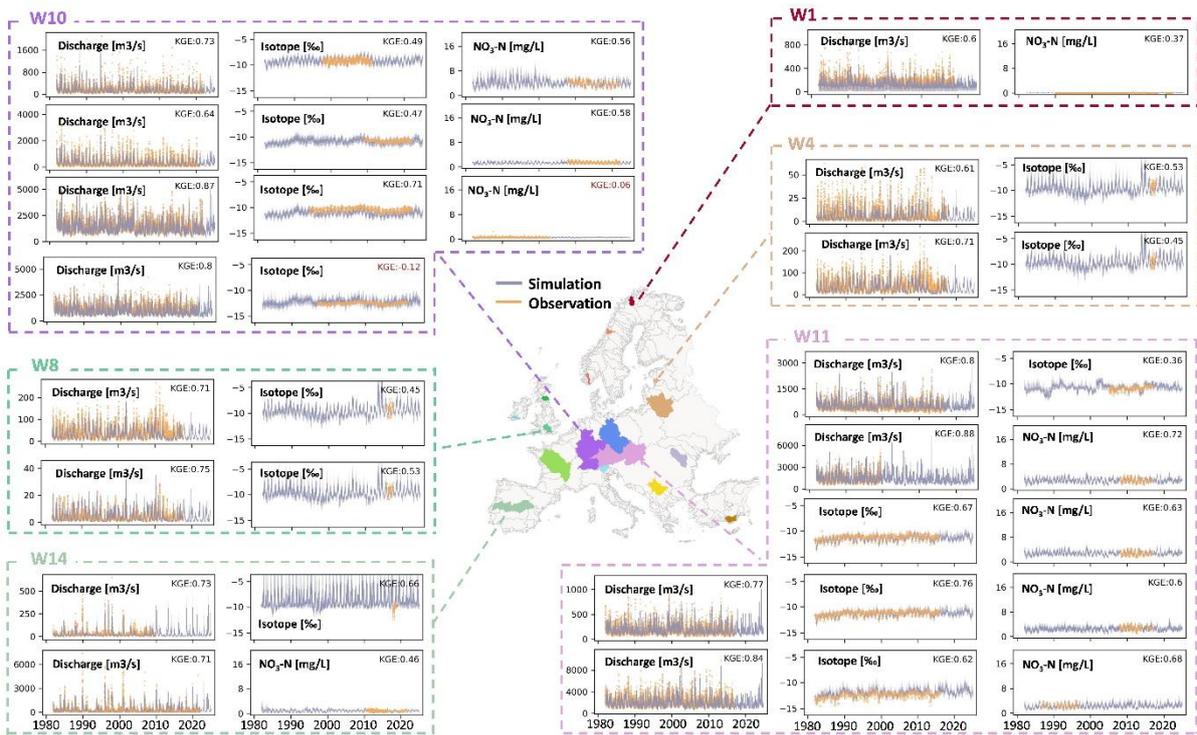
727

728

(a) Discharge simulation **(b) In-stream isotope simulation** **(c) In-stream NO$_3$-N simulation**
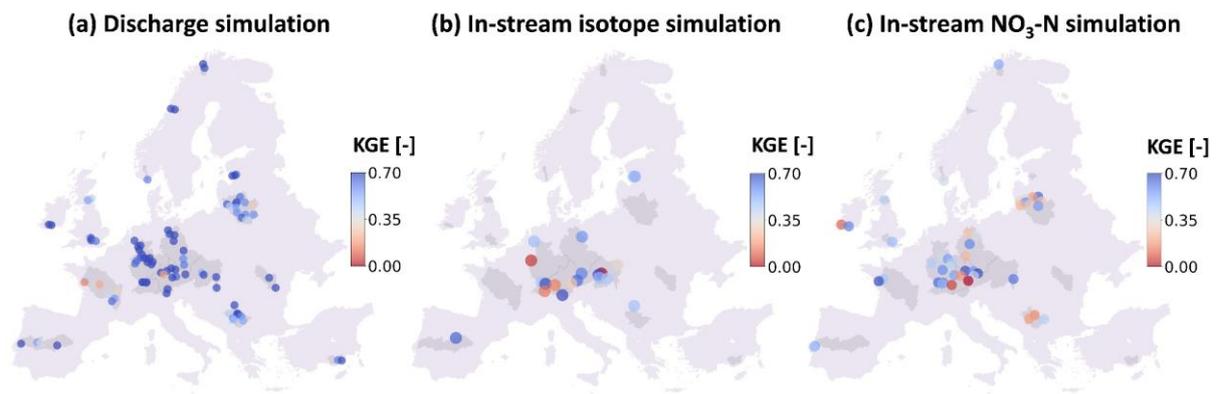
729

730   Figure 3. The simulation performance of discharge, in-stream isotope, and in-stream NO$_3$-N.

731

732

733

Figure 4. The simulated (blue) and observed (orange) time series of discharge, isotopes, and NO₃-N at representative gauges. Note that the sites with relatively poor performance (KGE < 0.2) were particularly shown for model diagnosis.
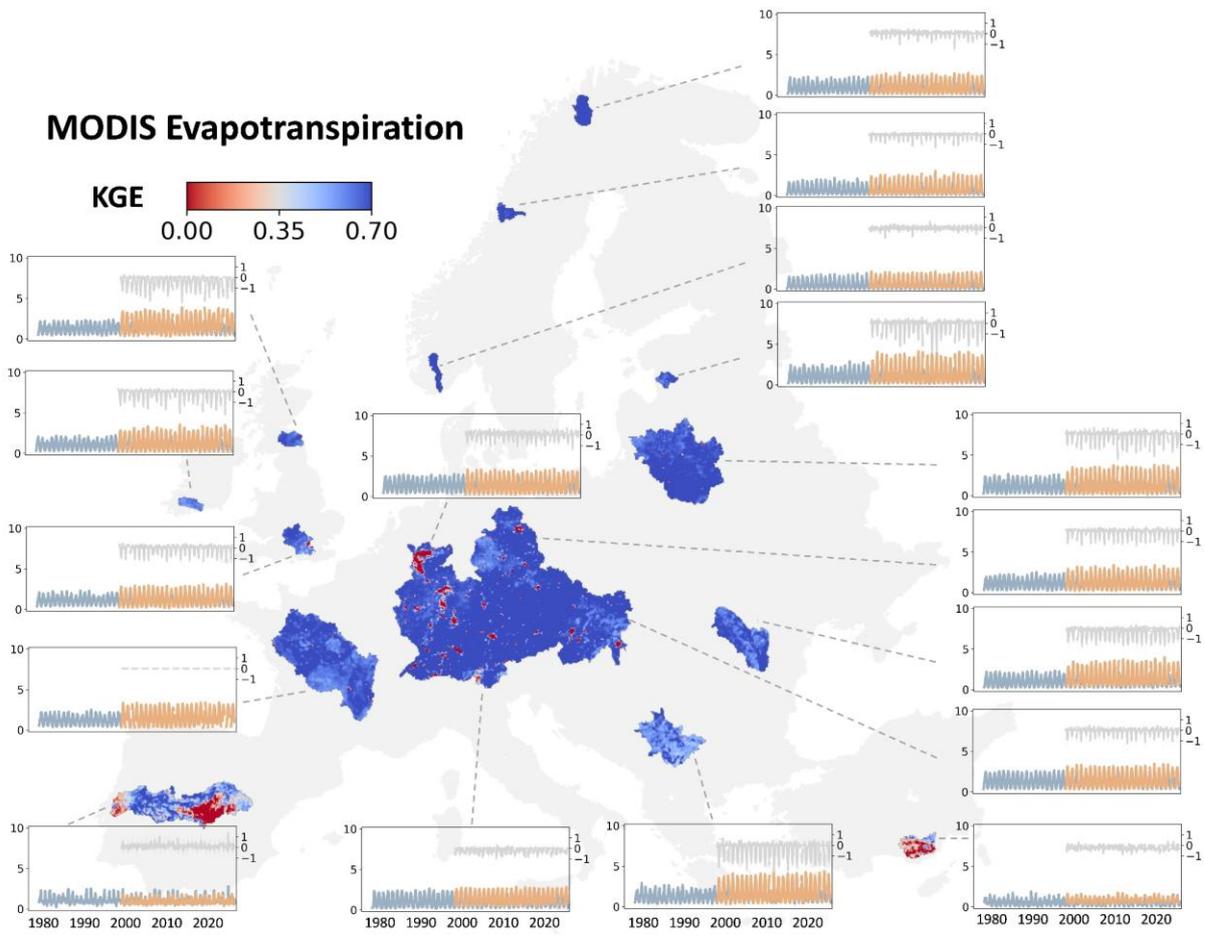
Figure 5. The grid-to-grid comparison between simulated evapotranspiration and MODIS evapotranspiration shown in KGE. The time series in inset subplots show the monthly dynamics of simulated (blue) and observed (orange) values averaged from all grid cells in the watershed, as well as their deviations (grey).
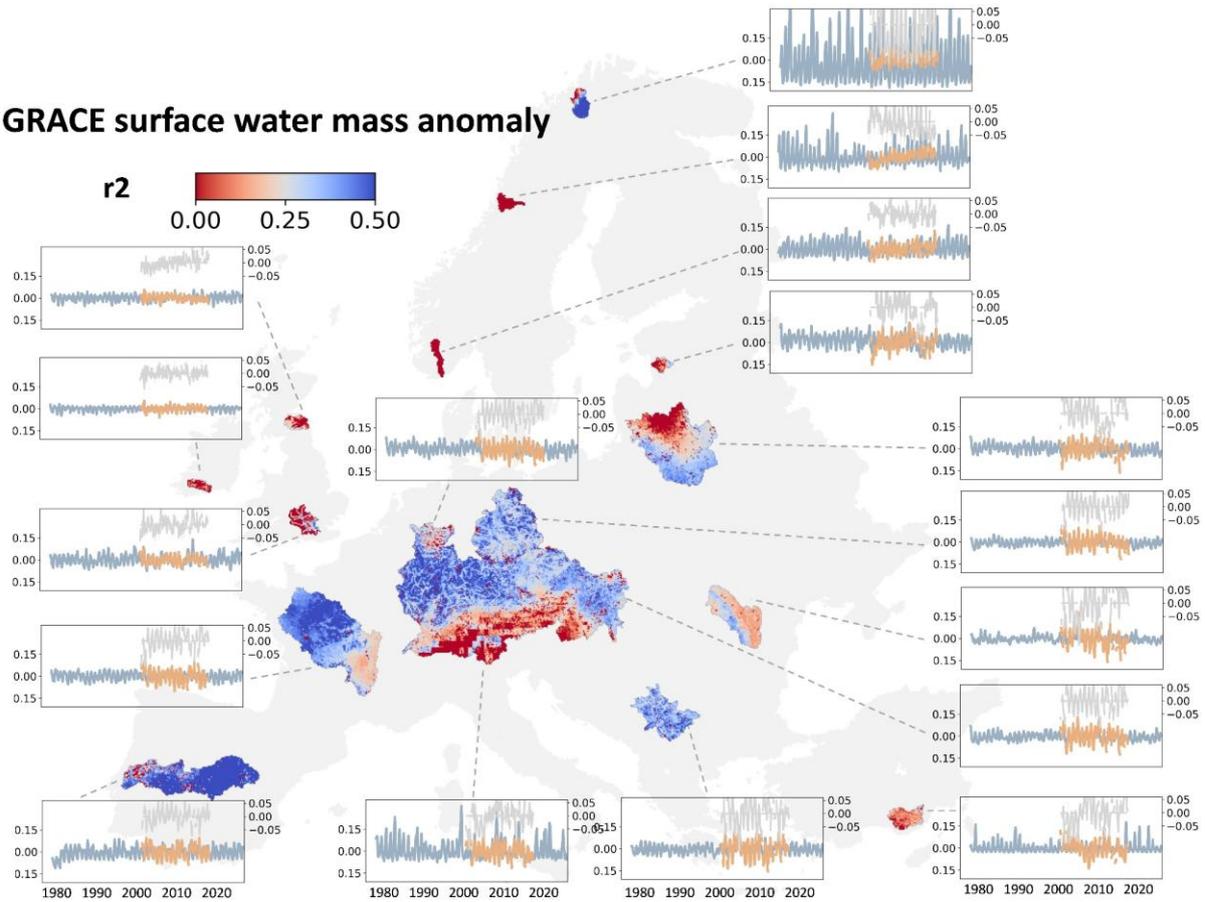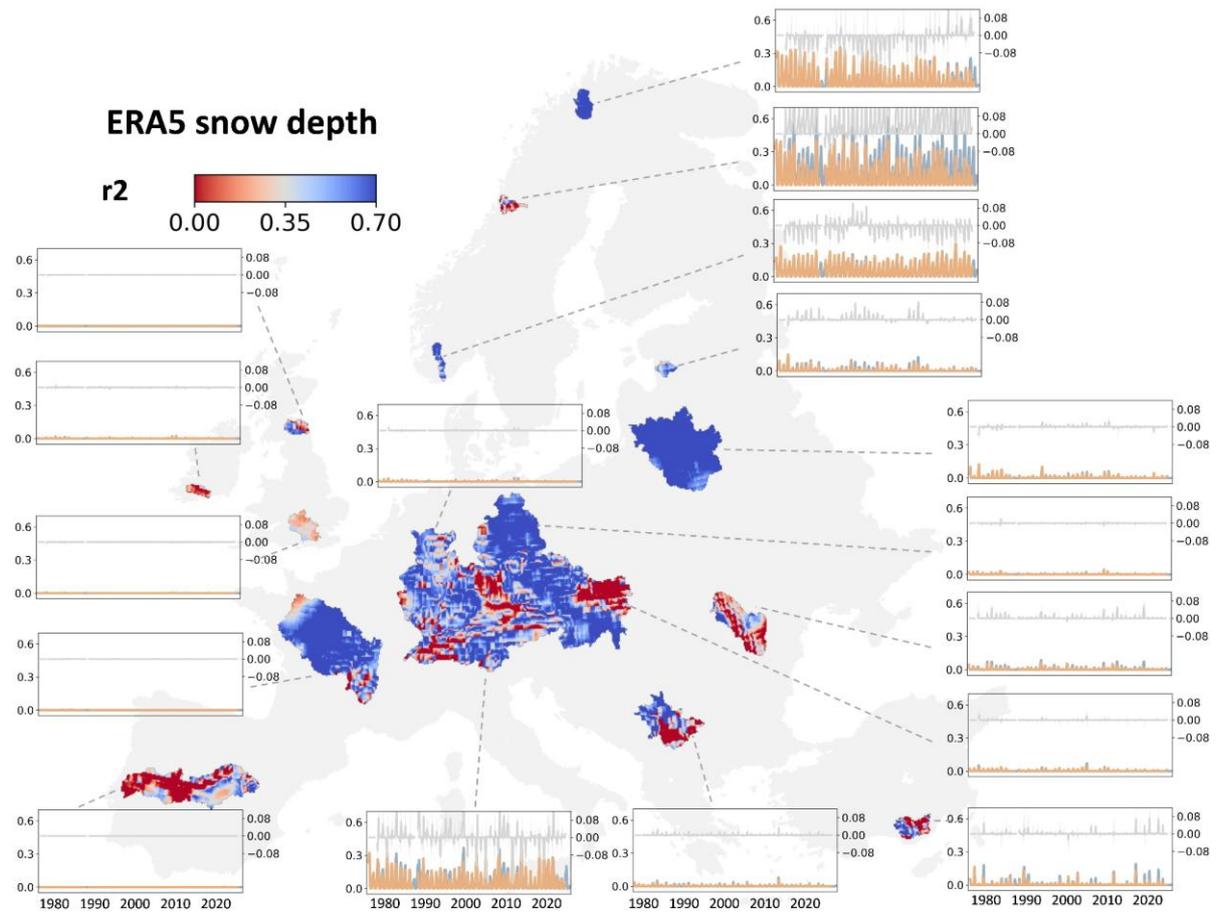
Figure 6. The grid-to-grid comparison between simulated water storage anomaly and GRACE surface water mass anomaly. The time series show the monthly dynamics of simulated (blue) and observed (orange) values averaged from all grid cells in the watershed, as well as their deviations (grey).

Figure 7. The grid-to-grid comparison between simulated snow depth and ERA5 snow depth. The time series show the monthly dynamics of simulated (blue) and observed (orange) values averaged from all grid cells in the watershed, as well as their deviations (grey).
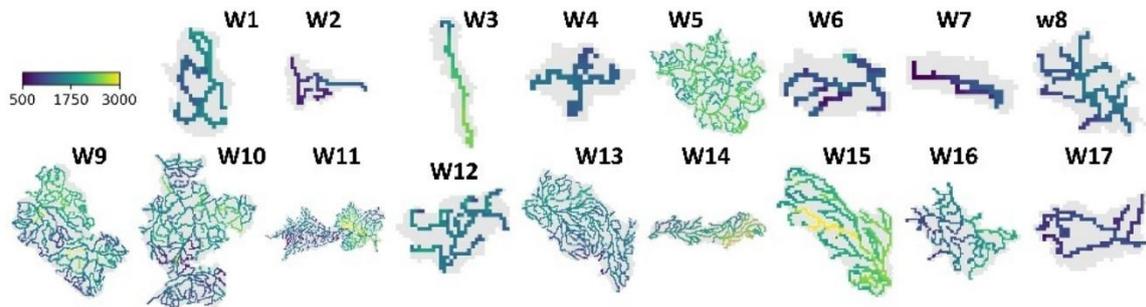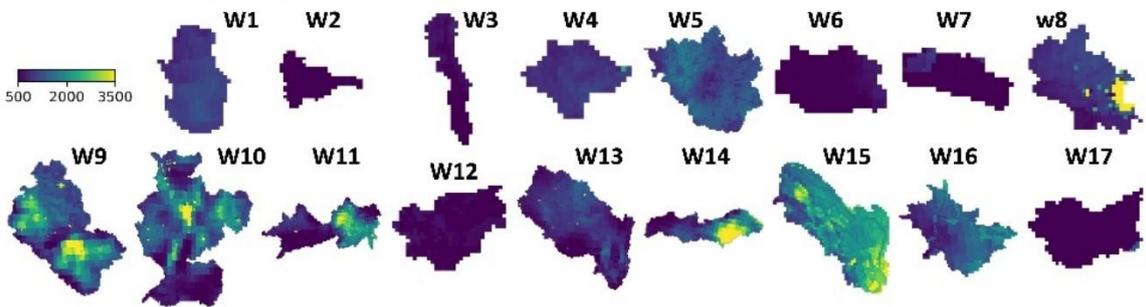
753
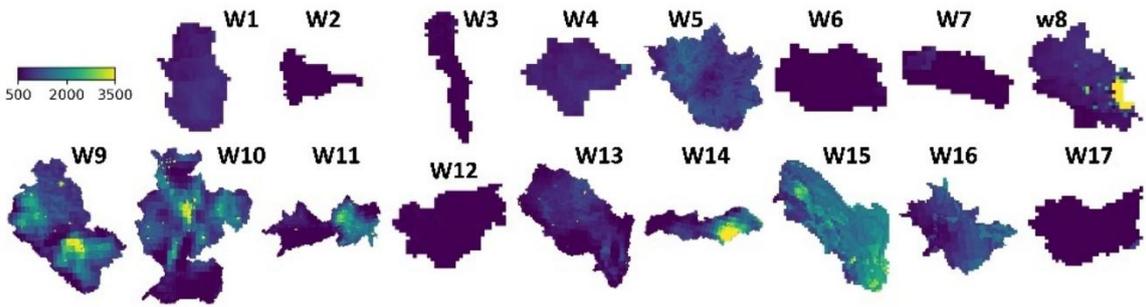
Figure 8. The simulated long-term average (1982-2024) of water age and travel time in channel and soil profile. Water ages represent the time since water enters the catchments as precipitation, while travel times depict the residence time of water within the specific storage.

758
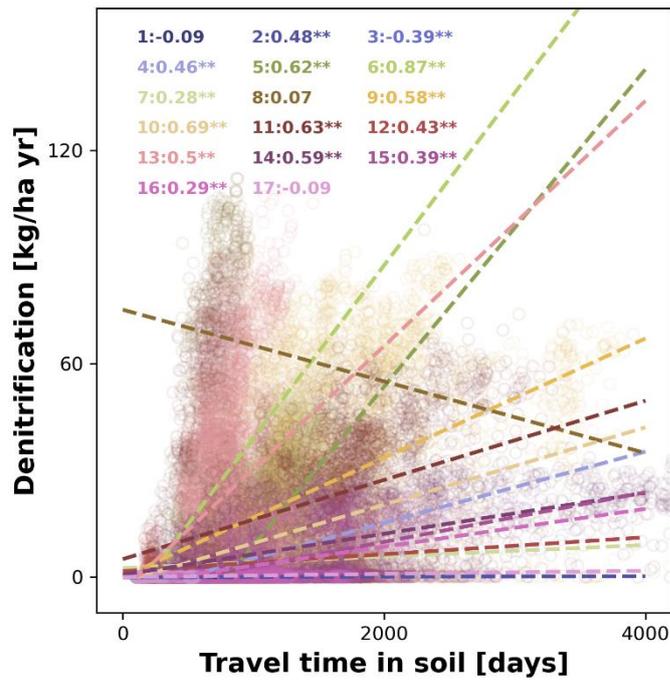
Figure 9. The correlations between travel time and annual denitrification. The text depicts the spearman correlation coefficients and p values (* = less than 0.05, ** = less than 0.01) in each catchment.

(a) Nitrogen inputs [kg/ha yr]
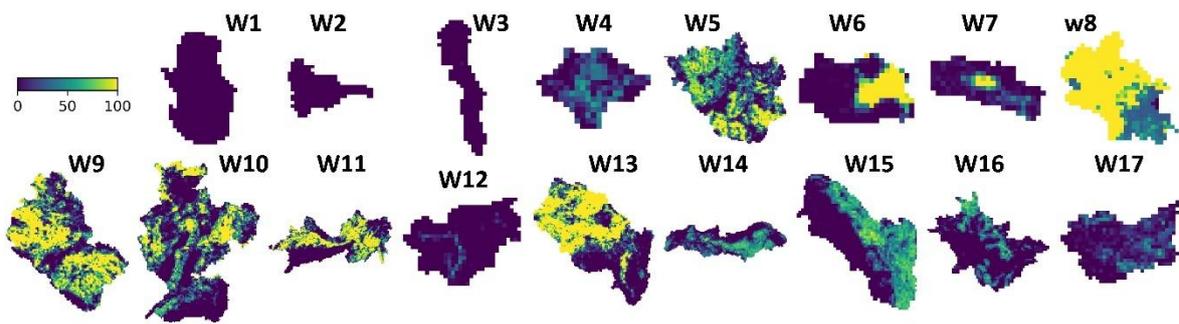
(b) Soil denitrification [kg/ha yr]
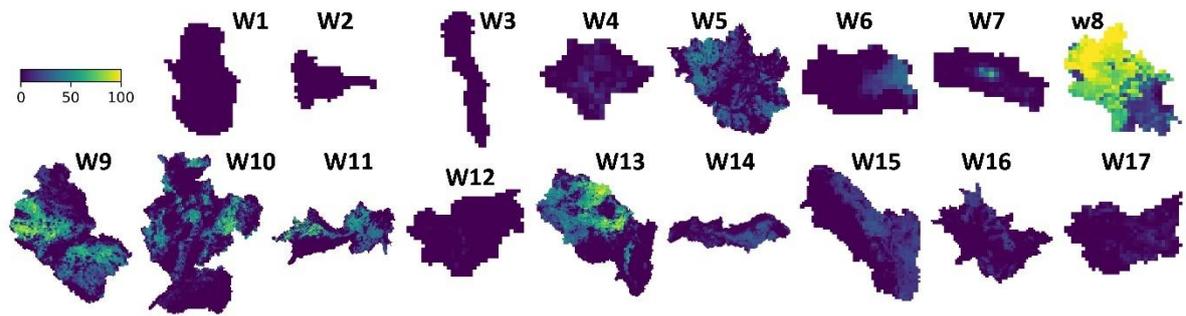
(c) Damköhler number [-]
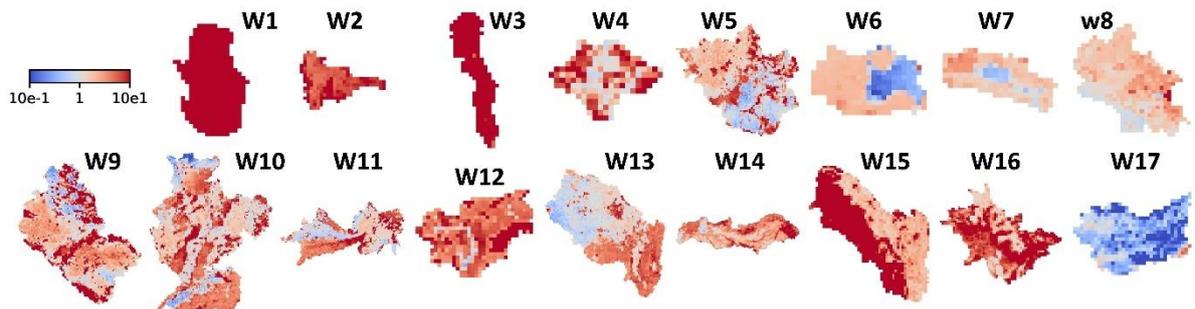
764

765 Figure 10. The simulated long-term average (1982-2024) of nitrogen inputs, soil denitrification, and

766 Damköhler number.

767

768

769 **Tables**

770 Table 1. Characteristics of the selected catchments. **Lat** depicts the latitude of upper left corner of the
771 catchment. **DEM** and **Area** are the mean elevation in m.a.s.l. and catchment size in km^2. **Precip**, **Temp**,
772 and **PET** are the annual averages of precipitation, air temperature, and potential evapotranspiration
773 in mm/yr. f_{crop}, f_{forest}, and f_{urban} are the fractions of cropland, forest, and urbanized areas in 2019
774 in %. Null means no name is assigned for the catchment in the Catchment Characterisation and
775 Modelling (CCM) database.

ID	Name	Lat	Area	DEM	Precip	Temp	PET	f_{crop}	f_{forest}	f_{urban}
1	Null	70.0	8725	468.5	448.5	-1.8	442.8	<1	1.9	<1
2	Vefsna	65.9	5475	636.5	1260.8	0.7	433.6	<1	24.6	<1
3	Null	59.8	5225	742.3	1400.9	3.0	545.7	<1	39.8	<1
4	Null	58.3	4350	67.4	654.5	6.4	667.9	17.4	60.5	1.4
5	Nemunas	56.6	97550	147.9	599.3	7.1	730.6	33.0	39.1	4.5
6	Tweed	55.9	6250	264.3	1023.4	7.9	600.9	21.8	18.9	1.4
7	Null	52.3	4300	175.4	1218.1	10.1	645.2	12.1	17.4	1.9
8	Thames	52.2	11900	112.0	700.7	10.4	782.9	44.9	14.1	22.0
9	Elbe	53.5	130225	318.3	626.9	8.8	836.3	41.2	34.6	10.8
10	Rhine	52.0	170175	508.3	943.3	8.9	821.0	21.5	41.2	17.1
11	Danube$_{(a)}$	50.5	197600	618.0	843.6	8.3	857.4	28.5	37.1	11.5
12	Adige	47.2	11600	1771.9	1002.3	4.5	809.7	<1	48.8	3.2
13	Loire	48.7	122125	298.9	778.7	11.0	887.4	37.6	25.7	6.5
14	Tajo	40.4	75575	686.2	549.5	14.3	1359.6	26.7	34.5	3.3
15	Danube$_{(b)}$	48.4	37975	533.3	534.7	8.1	869.5	32.0	41.3	6.4
16	Danube$_{(c)}$	44.8	37725	653.3	684.7	9.7	994.2	12.8	44.3	5.8
17	Null	37.6	12650	1384.5	454.1	12.2	1256.9	5.9	4.3	<1

776

777

778 Table 2. The calibration performance of discharge (Q), in-stream isotopes (^{18}O, Iso), and nitrate (NO^3-
779 N). Evaluation metrics include Kling-Gupta efficiency (KGE, -), Root Mean Square Error (RMSE; m3/s, ‰,
780 and mg/L for discharge, isotopes, and nitrate, respectively), Pearson Correlation Coefficient
781 (Coefficient; -), and Percent bias (Pbias; %).

Metric	Min	Max	Mean	Median
KGE (Q)	0.14	0.89	0.65	0.69
KGE (Iso)	-0.03	0.86	0.45	0.48
KGE (NO^3-N)	-0.36	0.72	0.42	0.44
Correlation (Q)	0.49	0.92	0.79	0.81
Correlation (Iso)	0.14	0.87	0.51	0.54
Correlation (NO^3-N)	-0.26	0.86	0.55	0.6
RMSE (Q)	3.99	677.08	123.02	68.51
RMSE (Iso)	0.31	1.51	0.72	0.73
RMSE (NO^3-N)	0.02	2.82	0.83	0.57
Pbias (Q)	0.52	79.88	17.44	9.53
Pbias (Iso)	-11.28	-0.07	-4.3	-4.42
Pbias (NO^3-N)	0.18	49.25	15.52	10.89

782

783

Reference

Akbarzadeh, Z., Maavara, T., Slowinski, S., & Van Cappellen, P. (2019). Effects of Damming on River Nitrogen Fluxes: A Global Analysis. *Global Biogeochemical Cycles*, *33*. https://doi.org/10.1029/2019GB006222

Ala-aho, P., Tetzlaff, D., Mcnamara, J., Laudon, H., & Kormos, P. (2017). Modeling the isotopic evolution of snowpack and snowmelt: Testing a spatially distributed parsimonious approach. *Water Resources Research*, *53*. https://doi.org/10.1002/2017WR020650

Amato, M. T., & Giménez, D. (2024). Predicting monthly near-surface soil temperature from air temperature and the leaf area index. *Agricultural and Forest Meteorology*, *345*, 109838. https://doi.org/10.1016/j.agrformet.2023.109838

Arnold, J., Moriasi, D., Gassman, P., Abbaspour, K., White, M., Srinivasan, R., et al. (2012). SWAT: Model use, calibration, and validation. *Transactions of the ASABE (American Society of Agricultural and Biological Engineers)*, *55*. https://doi.org/10.13031/2013.42256

Bajracharya, A., Moghairib, M., Stadnyk, T., & Asadzadeh, M. (2023). Process based calibration of a continental-scale hydrological model using soil moisture and streamflow data. *Journal of Hydrology: Regional Studies*, *47*, 101391. https://doi.org/10.1016/j.ejrh.2023.101391

Benettin, P., Bailey, S., Campbell, J., Green, M., Rinaldo, A., Likens, G., et al. (2015). Linking water age and solute dynamics in streamflow at the Hubbard Brook Experimental Forest, NH, USA. *Water Resources Research*, *51*, 9256–9272. https://doi.org/10.1002/2015WR017552

Beven, K. (2006). A manifesto for the equifinality thesis. *Journal of Hydrology*, *320*(1–2), 18–36. https://doi.org/10.1016/J.JHYDROL.2005.07.007

Beven, K. (2015). Facets of uncertainty: Epistemic uncertainty, non-stationarity, likelihood, hypothesis testing, and communication. *Hydrological Sciences Journal*, *61*, 150407155940006. https://doi.org/10.1080/02626667.2015.1031761

Birkel, C., & Soulsby, C. (2015). Advancing tracer-aided rainfall-runoff modelling: A review of progress, problems and unrealised potential. *Hydrological Processes*, *29*(25), 5227–5240. https://doi.org/10.1002/HYP.10594

Birkel, C., Tetzlaff, D., & Dunn, S. (2011). Using time domain and geographic source tracers to conceptualize streamflow generation processes in lumped rainfall-runoff models. *Water Resources Research - WATER RESOUR RES*, *47*. https://doi.org/10.1029/2010WR009547

Bonchkovskyi, A., & Osadcha, N. (2024). Modelling of the nutrient load in the Sula River basin using the MONERIS. *Physical Geography and Geomorphology*, *47*, 7–20. https://doi.org/10.17721/phgg.2024.3-4.01

Condon, L., Kollet, S., Bierkens, M., Maxwell, R., Hill, M., Franssen, H.-J., et al. (2021). Global Groundwater Modeling and Monitoring: Opportunities and Challenges. *Water Resources Research*, *57*. https://doi.org/10.1029/2020WR029500

Craig, H., Gordon, L. I., & Horibe, Y. (1964). Isotopic exchange effects in the evaporation of water: 1. Low-temperature experimental results. *Journal of Geophysical Research*, *68*(17), 5079–5087. https://doi.org/10.1029/JZ068I017P05079

Dawson, T., & Ehleringer, J. (1991). Streamside trees that do not use stream water. *Nature*, *350*, 335–337. https://doi.org/10.1038/350335a0

Dick, J. J., Tetzlaff, D., Birkel, C., & Soulsby, C. (2015). Modelling landscape controls on dissolved organic carbon sources and fluxes to streams. *Biogeochemistry*, *122*(2–3), 361–374. https://doi.org/10.1007/S10533-014-0046-3

Donnelly, C., Andersson, J. C. M., & Arheimer, B. (2016). Using flow signatures and catchment similarities to evaluate the E-HYPE multi-basin model across Europe. *Hydrological Sciences Journal*, *61*(2), 255–273. https://doi.org/10.1080/02626667.2015.1027710

831 Eckersten, H., Jansson, P. E., & Johnsson, H. (1994). SOILN model – user's manual 2nd edition, Division
832 of Agricultural Hydrotechnics Communications, 94:4. Department of Soil Sciences, Swedish
833 University of AgriculturalSciences, 58pp, Uppsala.

834 Efstratiadis, A., & Koutsoyiannis, D. (2010). One decade of multi-objective calibration approaches in
835 hydrological modelling: A review. *Hydrological Sciences Journal*, *55*(1), 58–78.
836 https://doi.org/10.1080/02626660903526292

837 Godsey, S. E., Aas, W., Clair, T. A., de Wit, H. A., Fernandez, I. J., Kahl, J. S., et al. (2010). Generality of
838 fractal 1/f scaling in catchment tracer time series, and its implications for catchment travel
839 time distributions. *Hydrological Processes*, *24*(12), 1660–1671.
840 https://doi.org/10.1002/hyp.7677

841 Good, S. P., Soderberg, K., Guan, K., King, E. G., Scanlon, T. M., & Caylor, K. K. (2014). δ2H isotopic flux
842 partitioning of evapotranspiration over a grass field following a water pulse and subsequent
843 dry down. *Water Resources Research*, *50*(2), 1410–1432.
844 https://doi.org/10.1002/2013WR014333

845 Grizzetti, B., Vigiak, O., Udias, A., Aloe, A., Zanni, M., Bouraoui, F., et al. (2021). How EU policies could
846 reduce nutrient pollution in European inland and coastal waters. *Global Environmental*
847 *Change*, *69*, 102281. https://doi.org/10.1016/j.gloenvcha.2021.102281

848 Hooper, R., Stone, A., Christophersen, N., de Melo, E., & Seip, H. (1988). Assessing the Birkenes Model
849 of Stream Acidification using a multi-signal calibration methodology. *Water Resources*
850 *Research - WATER RESOUR RES*, *24*, 1308–1316. https://doi.org/10.1029/WR024i008p01308

851 Horita, J., Rozanski, K., & Cohen, S. (2008). Isotope effects in the evaporation of water: A status report
852 of the Craig-Gordon model. *Isotopes in Environmental and Health Studies*, *44*, 23–49.
853 https://doi.org/10.1080/10256010801887174

854 Hrachowitz, M., Savenije, H., Bogaard, T. A., Tetzlaff, D., & Soulsby, C. (2013). What can flux tracking
855 teach us about water age distribution patterns and their temporal dynamics? *Hydrology and*
856 *Earth System Sciences*, *17*(2), 533–564. https://doi.org/10.5194/HESS-17-533-2013

857 Huijgevoort, M., Tetzlaff, D., & Sutanudjaja, E. (2016). Using high resolution tracer data to constrain
858 water storage, flux and age estimates in a spatially distributed rainfall-runoff model.
859 *Hydrological Processes*, *30*. https://doi.org/10.1002/hyp.10902

860 Jasechko, S., Kirchner, J., Welker, J., & McDonnell, J. (2016). Substantial proportion of global
861 streamflow less than three months old. *Nature Geoscience*, *9*.
862 https://doi.org/10.1038/NGEO2636

863 Jones, E. R., Bierkens, M. F. P., Wanders, N., Sutanudjaja, E. H., van Beek, L. P. H., & van Vliet, M. T. H.
864 (2023). DynQual v1.0: a high-resolution global surface water quality model. *Geoscientific*
865 *Model Development*, *16*(15), 4481–4500. https://doi.org/10.5194/gmd-16-4481-2023

866 Jung, H., Tetzlaff, D., Birkel, C., & Soulsby, C. (2025). Recent Developments and Emerging Challenges
867 in Tracer-Aided Modeling. *Wiley Interdisciplinary Reviews Water*, *12*.
868 https://doi.org/10.1002/wat2.70015

869 Kale, R., & Sahoo, B. (2011). Green-Ampt Infiltration Models for Varied Field Conditions: A Revisit.
870 *Water Resources Management*, *25*, 3505–3536. https://doi.org/10.1007/s11269-011-9868-0

871 Kumar, R., Samaniego, L., & Attinger, S. (2013). Implications of distributed hydrologic model
872 parameterization on water fluxes at multiple scales and locations. *Water Resources Research*,
873 *49*(1), 360–379. https://doi.org/10.1029/2012WR012195

874 Kuppel, S., Tetzlaff, D., Maneta, M., & Soulsby, C. (2018). EcH2O-iso 1.0: Water isotopes and age
875 tracking in a process-based, distributed ecohydrological model. *Geoscientific Model*
876 *Development*, *11*, 3045–3069. https://doi.org/10.5194/gmd-11-3045-2018

877 Landgraf, J., Tetzlaff, D., Birkel, C., Stevenson, J., & Soulsby, C. (2023). Assessing land use effects on
878   ecohydrological partitioning in the critical zone through isotope-aided modelling. *Earth*
879   *Surface Processes and Landforms*, *48*. https://doi.org/10.1002/esp.5691

880 Lindström, G., Pers, C., Rosberg, J., Strömqvist, J., & Arheimer, B. (2010). Development and test of the
881   HYPE (Hydrological Predictions for the Environment) model – A water quality model for
882   different spatial scales. *Hydrology Research*, *41*. https://doi.org/10.2166/nh.2010.007

883 Maneta, M. P., & Silverman, N. L. (2013). A spatially distributed model to simulate water, energy, and
884   vegetation dynamics using information from regional climate models. *Earth Interactions*,
885   *17*(11), 1–44. https://doi.org/10.1175/2012EI000472.1

886 McDonnell, J. (2014). The two water worlds hypothesis: Ecohydrological separation of water between
887   streams and trees? *Wiley Interdisciplinary Reviews: Water*, *1*.
888   https://doi.org/10.1002/wat2.1027

889 McDonnell, J., & Beven, K. (2014). Debates on Water Resources: The future of hydrological sciences:
890   A (common) path forward? A call to action aimed at understanding velocities, celerities and
891   residence time distributions of the headwater hydrograph. *Water Resources Research*, *50*.
892   https://doi.org/10.1002/2013WR015141

893 Mcmillan, H., Araki, R., Bolotin, L., Kim, D.-H., Coxon, G., Clark, M., & Seibert, J. (2025). Global patterns
894   in observed hydrologic processes. *Nature Water*, *3*. https://doi.org/10.1038/s44221-025-
895   00407-w

896 Mikayilov, F., Rouholahnejad Freund, E., Ashraf Vaghefi, S., Srinivasan, R., Yang, H., & Klöve, B. (2015).
897   A continental-scale hydrology and water quality model for Europe: Calibration and uncertainty
898   of a high-resolution large-scale SWAT model. *Journal of Hydrology*, *524*.
899   https://doi.org/10.1016/j.jhydrol.2015.03.027

900 Nan, Y., He, Z., Tian, F., Wei, Z., & Tian, L. (2021). Can we use precipitation isotope outputs of isotopic
901   general circulation models to improve hydrological modeling in large mountainous
902   catchments on the Tibetan Plateau? *Hydrology and Earth System Sciences*, *25*(12), 6151–6172.
903   https://doi.org/10.5194/hess-25-6151-2021

904 Naz, B. S., Sharples, W., Ma, Y., Goergen, K., & Kollet, S. (2023). Continental-scale evaluation of a fully
905   distributed coupled land surface and groundwater model, ParFlow-CLM (v3.6.0), over Europe.
906   *Geoscientific Model Development*, *16*(6), 1617–1639. https://doi.org/10.5194/gmd-16-1617-
907   2023

908 Neal, C., Christophersen, N., Neale, R., Smith, C., & Reynolds, B. (1988). Chloride in precipitation and
909   streamwater for the upland catchment of River Severn, mid- Wales; some consequences for
910   hydrochemical models. *Hydrological Processes*, *2*, 155–165.
911   https://doi.org/10.1002/hyp.3360020206

912 Nearing, G., Ruddell, B., Bennett, A., Prieto, C., & Gupta, H. (2020). Does Information Theory Provide
913   a New Paradigm for Earth Science? Hypothesis Testing. *Water Resources Research*, *56*.
914   https://doi.org/10.1029/2019WR024918

915 Ocampo, C., Sivapalan, M., & Oldham, C. (2006). Hydrological connectivity of upland-riparian zones in
916   agricultural catchments: Implications for runoff generation and nitrate transport. *Journal of*
917   *Hydrology*, *331*, 643–658. https://doi.org/10.1016/j.jhydrol.2006.06.010

918 Pechlivanidis, I., Jackson, B., Mcintyre, N., & Wheater, H. (2011). Catchment scale hydrological
919   modelling: A review of model types, calibration approaches and uncertainty analysis methods
920   in the context of recent developments in technology and applications. *GlobalNEST*
921   *International Journal*, *13*, 193–214.

922 Pesántez, J., Birkel, C., Gaona, G., Arciniega-Esparza, S., Murray, D., Mosquera, G., et al. (2023).
923   Spatially distributed tracer-aided modelling to explore DOC dynamics, hot spots and hot
924   moments in a tropical mountain catchment. *Hydrological Processes*, *37*, 1–15.
925   https://doi.org/10.1002/hyp.15020

Rakovec, O., Kumar, R., Mai, J., Cuntz, M., Thober, S., Zink, M., et al. (2016). Multiscale and Multivariate Evaluation of Water Fluxes and States over European River Basins. *Journal of Hydrometeorology*, *17*, 287–307. https://doi.org/10.1175/JHM-D-15-0054.1

Rakovec, O., Mizukami, N., Kumar, R., Newman, A., Thober, S., Wood, A., et al. (2019). Diagnostic Evaluation of Large-Domain Hydrologic Models Calibrated Across the Contiguous United States. *Journal of Geophysical Research: Atmospheres*, *124*. https://doi.org/10.1029/2019JD030767

Remondi, F., Kirchner, J., Burlando, P., & Fatichi, S. (2018). Water Flux Tracking with A Distributed Hydrological Model to Quantify Controls on the Spatio-Temporal Variability of Transit Time Distributions. *Water Resources Research*, *54*. https://doi.org/10.1002/2017WR021689

Samaniego, L., Kumar, R., & Attinger, S. (2010). Multiscale parameter regionalization of a grid-based hydrologic model at the mesoscale. *Water Resour. Res.*, *46*. https://doi.org/10.1029/2008WR007327

Seybold, E., Dwivedi, R., Musselman, K., Kincaid, D., Schroth, A., Classen, A., et al. (2022). Winter runoff events pose an unquantified continental-scale risk of high wintertime nutrient export. *Environmental Research Letters*, *17*, 104044. https://doi.org/10.1088/1748-9326/ac8be5

Šimůnek, J., Šejna, M., Saito, H., & Van Genuchten, M. T. (2013). *The HYDRUS-1D software package for simulating the one-dimensional movement of water, heat, and multiple solutes in variably-saturated media (Version 4.17)*. Department of Environmental Sciences University of Riverside California, California.

Skrzypek, G., Mydłowski, A., Dogramaci, S., Hedley, P., Gibson, J. J., & Grierson, P. F. (2015). Estimation of evaporative loss based on the stable isotope composition of water using Hydrocalculator. *Journal of Hydrology*, *523*, 781–789. https://doi.org/10.1016/J.JHYDROL.2015.02.010

Smith, A., Tetzlaff, D., Kleine, L., Maneta, M., & Soulsby, C. (2021). Quantifying the effects of land use and model scale on water partitioning and water ages using tracer-aided ecohydrological models. *Hydrology and Earth System Sciences*, *25*, 2239–2259. https://doi.org/10.5194/hess-25-2239-2021

Soulsby, C., Birkel, C., Geris, J., Dick, J., Tunaley, C., & Tetzlaff, D. (2015). Stream water age distributions controlled by storage dynamics and nonlinear hydrologic connectivity: Modeling with high-resolution isotope data. *Water Resources Research*, *51*(9), 7759–7776. https://doi.org/10.1002/2015WR017888

Sprenger, M., Stumpp, C., Weiler, M., Aeschbach, W., Allen, S., Benettin, P., et al. (2019). The Demographics of Water: A Review of Water Ages in the Critical Zone. *Reviews of Geophysics*, *57*. https://doi.org/10.1029/2018RG000633

Tetzlaff, D., Buttle, J., Carey, S. K., Mcguire, K., Laudon, H., & Soulsby, C. (2015). Tracer-based assessment of flow paths, storage and runoff generation in northern catchments: A review. *Hydrological Processes*, *29*(16), 3475–3490. https://doi.org/10.1002/HYP.10412

Wang, J., Bouwman, A., Vilmin, L., Beusen, A., Hoek, W., Liu, X., & Middelburg, J. (2024). Global inland-water nitrogen cycling has accelerated in the Anthropocene. *Nature Water*, *2*. https://doi.org/10.1038/s44221-024-00282-x

Wellen, C., Kamran-Disfani, A.-R., & Arhonditsis, G. (2015). Evaluation of the Current State of Distributed Watershed Nutrient Water Quality Modeling. *Environmental Science & Technology*, *49*. https://doi.org/10.1021/es5049557

Wen, Y., Lin, J.-S., Plaza, F., & Liang, X. (2024). Roles of Hydrology and Transport Processes in Denitrification at Watershed Scale. *Water Resources Research*, *60*, 1–24. https://doi.org/10.1029/2023WR034971

972 Winkler, K., Fuchs, R., Rounsevell, M., & Herold, M. (2021). Global land use changes are four times
973 greater than previously estimated. *Nature Communications*, *12*(1), 2501.
974 https://doi.org/10.1038/s41467-021-22702-2

975 Wu, S., Tetzlaff, D., Yang, X., & Soulsby, C. (2022). Disentangling the influence of landscape
976 characteristics, hydroclimatic variability and land management on surface water NO_3-N
977 dynamics: spatially distributed modelling over 30 years in a lowland mixed land use catchment.
978 *Water Resources Research*, e2021WR030566. https://doi.org/10.1029/2021WR030566

979 Wu, S., Tetzlaff, D., Beven, K., & Soulsby, C. (2025a). DREAM(LoAX): Simultaneous Calibration and
980 Diagnosis for Tracer-Aided Ecohydrological Models Under the Equifinality Thesis. *Water*
981 *Resources Research*, *61*, e2024WR038779. https://doi.org/10.1029/2024WR038779

982 Wu, S., Tetzlaff, D., Yang, X., Sauter, T., & Soulsby, C. (2025b). Hydrological Connectivity Dominates
983 NO3-N Cycling in Complex Landscapes – Insights From Integration of Isotopes and Water
984 Quality Modeling. *Water Resources Research*, *61*, e2025WR040525.
985 https://doi.org/10.1029/2025WR040525

986 Wu, S., Tetzlaff, D., & Soulsby, C. (2025c). Revising Common Approaches for Calibration: Insights From
987 a 1-D Tracer-Aided Hydrological Model With High-Dimensional Parameters and Objectives.
988 *Water Resources Research*, *61*, e2024WR037656. https://doi.org/10.1029/2024WR037656

989 Wu, S., Tetzlaff, D., Zheng, Y., & Soulsby, C. (2025d). EcoTWIN v1.0 release.
990 https://doi.org/10.5281/zenodo.16747633

991 Yang, C., Condon, L., & Maxwell, R. (2025). Unravelling groundwater–stream connections over the
992 continental United States. *Nature Water*, *3*. https://doi.org/10.1038/s44221-024-00366-8

993 Yang, X., Jomaa, S., Zink, M., Fleckenstein, J., Borchardt, D., & Rode, M. (2018). A New Fully Distributed
994 Model of Nitrate Transport and Removal at Catchment Scale. *Water Resources Research*, *54*.
995 https://doi.org/10.1029/2017WR022380

996 Yang, X., Zhang, X., Graeber, D., Hensley, R., Jarvie, H., Lorke, A., et al. (2023a). Large-stream nitrate
997 retention patterns shift during droughts: Seasonal to sub-daily insights from high-frequency
998 data-model fusion. *Water Research*, *243*, 120347.
999 https://doi.org/10.1016/j.watres.2023.120347

1000 Yang, X., Tetzlaff, D., Müller, C., Knöller, K., Borchardt, D., & Soulsby, C. (2023b). Upscaling Tracer-
1001 Aided Ecohydrological Modeling to Larger Catchments: Implications for Process
1002 Representation and Heterogeneity in Landscape Organization. *Water Resources Research*, *59*,
1003 e2022WR033033. https://doi.org/10.1029/2022WR033033

1004 Yang, X., Tetzlaff, D., Jin, J., Li, Q., Borchardt, D., & Soulsby, C. (2024). Linking terrestrial biogeochemical
1005 processes and water ages to catchment water quality: A new Damköhler analysis based on
1006 coupled modeling of isotope tracers and nitrate dynamics. *Water Research*, *262*, 122118.
1007 https://doi.org/10.1016/j.watres.2024.122118

1008 Zhang, Z., Chen, X., Cheng, Q.-B., Li, S.-L., Yue, F.-J., Peng, T., et al. (2020). Coupled hydrological and
1009 biogeochemical modelling of nitrogen transport in the karst critical zone. *Science of The Total*
1010 *Environment*, *732*, 138902. https://doi.org/10.1016/j.scitotenv.2020.138902

1011 Zhu, J., Jia, Y., Yu, G., Wang, Q., He, N., Chen, Z., et al. (2025). Changing patterns of global nitrogen
1012 deposition driven by socio-economic development. *Nature Communications*, *16*(1), 46.
1013 https://doi.org/10.1038/s41467-024-55606-y

1014